



Drag Reduction System

Spartan Racing Formula SAE

San Jose State University

Mechanical Engineering Department

ME 195B Final Report

May 9, 2022

Advisor: Dr. Raghu Agarwal

Authors: Josue E. Garcia, Scott R. Dunn, Jie Kai Teo, Junlin Chen, Ehsan Al-Agtash

Executive Summary

The Drag Reduction System (DRS for short) is a commonly adapted design on motor racing vehicles that aims to reduce the drag force while running down a straight racing track for an increased top speed and overtaking. This project recreates and implements the typical design of the DRS on the Spartan Racing (Formula SAE) student race car. The project incorporates the major disciplines of Mechatronic Engineering, which are Mechanical, Electrical, and Software Engineering.

The team was able to construct a driver-oriented design capable of alternating the state of the vehicle's spoiler to limit or promote air flowing through the rear wing. The design incorporates a rotary switch that will be used to select the different modes or methods of actuation. The major two modes of DRS are Manual and Automatic. The manual mode allows the driver to actuate the DRS whenever the driver presses on a momentary switch. The automatic mode will actuate the DRS automatically when a set of sensor parameters are matched. When the values of sensors, like steering angle and throttle position, are calculated so that the car is driving down a straight course, the drag reduction system will activate autonomously to increase the efficiency and speed of the speed.

The team implemented a mechanical linkage system to actuate DRS. These linkages, made of lightweight sheet metal, open and close the lower two rear wing flaps on the vehicle's spoiler to promote airflow or downforce. A spring returning mechanism was introduced in this project as a supplement to the actuator's returning mechanism. The spring, designed as a failsafe mechanism, was able to retract the pneumatic piston in the cases where the pneumatic system malfunctioned and the DRS was stuck in the opened state. The team was able to determine the efficiency and feasibility of different models of actuators by using an efficiency matrix and selected the most appropriate actuator for the DRS. The chosen actuator for this project is the BIMBA 022-DXP Pneumatic Piston.

A variety of sensors available on Spartan Racer 13 (SR13) was implemented in the Drag Reduction System's design. Sensors include throttle position, steering angle, brake pressure, and the Inertial Measurement Unit (IMU). The team managed to collect sensor data from the car's Electronic Control Unit (ECU) and Data Acquisition Unit (DAQ). From the data, the team was able to determine the validity of each sensor in terms of actuating the DRS. Using the analyzed data, the team created a set of codes in MoTeC M1 Build, a software recognized by the car's Electronic Control Unit. The final code was tested and the pneumatic piston was able to actuate when the momentary button (manual) or sensor conditions (automatic) were met.

In terms of manufacturing, the team machined a clevis meant to be mounted on the end of the actuating piston, with the use of a lathe and a milling device. The mechanical linkages of the DRS were made and cut out of 6061 Aluminum sheet metals. The mounts of the DRS accessories such as the air bottles, the solenoid, and the pneumatic piston were made and cut out of 4130 Alloy-Steel sheet metals. The rear wing end caps and flap mounts were manufactured through FDM 3D printing with Carbon Fiber Nylon as the material. The overall rigidity of the entire DRS assembly was satisfactory.

Acknowledgments

The Drag Reduction System (DRS) team would like to give credit to the rest of the Spartan Racing SJSU Formula SAE team for helping us throughout our design and manufacturing phase. The DRS team would like to acknowledge the effort and guidance of the Aerodynamics and Vehicle Dynamics team from Spartan Racing. The DRS team also would like to thank Dr. Raghu Agarwal for helping with feedback and suggestions during presentations. Additionally, The DRS team would like to give thanks to our sponsors, SMC Corporation of America and Buchanan Automation, Inc. for providing us with the equipment and materials we need to make the project a success. Some of the equipment provided include but are not limited to the pneumatic pistons, the air-line tubings, and the pneumatic solenoid valves.

Table of Contents

Executive Summary	1
Acknowledgments	3
Table of Contents	4
List of Figures	6
List of Tables	9
Nomenclature	10
1. Introduction	13
1.1 Design Backgrounds	13
1.2 Design Objectives & Specifications	15
1.3 Literature Review	17
2. Theory	19
2.1 Angle of Attack and Drag Force	19
2.2 Hooke's Law	20
2.3 Linear and Rotary Position Sensor	21
3. Design	23
3.1 Mechanical Design	23
3.1.1 CFD Data Analysis	23
3.1.2 Rear Wing Foil Sleeve Design	24
3.1.3 Rear Wing End Caps Design	26
3.1.4 Mechanical Linkage Design	27
3.1.5 4-bar Linkage design	29
3.1.7 Piston Clevis Design	33
3.1.8 Air Bottle Mounting	34
3.1.9 Return Spring Design	39

3.2 Controls Design	42
3.2.1 Sensor Data Analysis	42
3.2.2 Sensor Selection	43
3.2.3 Actuation Methods Analysis	44
3.2.4 Actuator Selection	45
3.2.5 Pneumatic System Design	47
3.2.6 Circuit Wiring & Control Diagrams	50
3.2.7 MoTec Software Programming	51
3.3 Manufacturing and Assembly	52
3.3.1 Parts Manufacturing	52
3.3.2 Component Assembly	54
3.4 Cost Analysis	60
4. Testing, Results, and Discussion	61
4.1 Test Results	61
4.2 Actuation Limit	62
4.3 Lap Simulation	64
4.4 Social Impacts	65
5. Conclusions and Future Work	67
References	68
Appendix	71
Appendix A: Simulations	71
Appendix B: Hardware	73
Appendix C: Software	77
Appendix D: Miscellaneous	79
Appendix E: MoTeC Code	80

List of Figures

Figure 1: Typical DRS configuration on a Formula 1 vehicle

Figure 2: Steering wheel of the Sauber C33 Formula 1 vehicle

Figure 3: Track Map Example showing the Optimum 'DRS Zone' on Straight Paths

Figure 4: Illustration showing the angle of attack and directions of lift and drag force

Figure 5: Graph of Angle-of-Attack against Lift and Drag force

Figure 6: Schematic diagram of a potentiometer

Figure 7: Computational fluid dynamics analysis of the rear wing

Figure 8: Foil sleeves 3D-printed using carbon fiber nylons

Figure 9: Foil sleeves assembled on the rear wing airfoils

Figure 10: End caps 3D-printed in Carbon-Fiber Nylon

Figure 11: Bonded end caps on the side of the DRS airfoils

Figure 12: linear pneumatic piston actuated four-bar linkage mechanism diagram.

Figure 13: SolidWorks CAD of Mechanism Kinematic Sketch

Figure 14: SolidWorks CAD Demonstration of the Transmission Angles

Figure 15: Efficiency vs. Actuator total length graph

Figure 16: Upstroke efficiency vs. Actuator total length graph

Figure 17: Downstroke efficiency vs. Actuator total length graph

Figure 18: Sheet metal rear wing foil mount shown in CAD

Figure 19: Sheet metal rear wing foil mount test fit on rear wing foil

Figure 20: Solidworks finite element analysis factor of safety plot

Figure 21: Solidworks finite element analysis bucking plot

Figure 22: Air bottle mount SolidWorks part model with hose clamp fitting

Figure 23: Air bottle mount (highlighted in pink) location on the combustion car

Figure 24: Air bottle mount (highlighted in pink) location on the electric car

Figure 25: Air bottle mount assembly exploded view

Figure 26: Air bottle mount with air bottle secured

Figure 27: Proposed return spring design (first version)

Figure 28: Revised return spring design (second version)

Figure 29: I2 Pro Data Analysis from Michigan with Track Overlay

Figure 30: BIMBA 022-DXP Pneumatic Piston

Figure 31: SMC 5 Port Solenoid Valve

Figure 32: SMC 5 Port Solenoid Valve CAD part

Figure 33: System Overview

Figure 34: System Overview

Figure 35: Open & close graph

Figure 36: Block Diagram

Figure 37: Sheet metal order of the mechanical linkages

Figure 38: Air bottle holder printed with PET-G plastic filaments

Figure 39: Machined clevis using a lathe

Figure 40: Installing the foil sleeves and linkage on the airfoils

Figure 41: Installing the main element and end plate on the sides

Figure 42: Installing the pneumatic piston and the return spring

Figure 43: Real-life assembly of the rear wing with DRS attached

Figure 44: Pneumatic system connection and setup

Figure 45: Electrical system connection and setup

Figure 46: Driver Accelerating Through Straight Track Section with DRS Actuated

Figure 47: Arduino code setup

Figure 48: Circuit setup for testing

Figure 49: LabVIEW VI for the DRS Lap Simulator

Figure 50: Calibration analysis of the throttle position sensor

Figure 51: Return spring constant analysis and calculation

Figure 52: SolidWorks drawing of the piston clevis

Figure 53: Automotive Software Process Improvement and Capability Determination (ASPICE) Framework of Drag Reduction System

Figure 54: M1 Tune

Figure 55: M1 Build

Figure 56: Formula SAE rules concerning the Drag Reduction System

List of Tables

Table 1: CFD results at a 0-degree angle of attack and 55 mph

Table 2: Actuator Decision Matrix with Scores per Category

Table 3: Bill of Material (BoM)

Table 4: Max number of actuation results

Table 5: Rear Wing Drag and Downforce Analysis at different AoA

Table 6: CFD results of different rear wing configurations at 55 mph

Table 7: Decision matrix for actuation method analysis

Table 8: Piston selection analysis

Table 9: Sensor validation and analysis

Table 10: 4-bar linkage calculations

Table 11: 4-bar linkage calculations

Nomenclature

AoA	Angle of Attack
BIMBA	Actuator company (brand of piston)
BoM	Bill of Materials
CAD	Computer-Aided Design
CAN	Controller Area Network
CDR	Concept Design Review
CF	Carbon Fiber
CFD	Computational Fluid Dynamics
CFN	Carbon Fiber Nylon
CG	Center of Gravity
CNC	Computer Numerical Control
CoP	Center of Pressure
DAQ	Data Acquisition Device
DDR	Detailed Design Review
DF	Downforce
DRS	Drag Reduction System
ECU	Electronic Control Unit
FEA	Finite Element Analysis

FSAE	Formula Society of Automotive Engineers
IMU	Inertial Measurement Unit
MoTeC	Motorsports Technology - Brand of the Electronic Control Unit
MoTeC i2Pro	Data Analysis Software of the Electronic Control Unit
MoTeC M150	Model Number of the Electronic Control Unit
MoTeC M1 Build	Programming Software of the Electronic Control Unit
MoTeC M1 Tune	Tuning Software of the Electronic Control Unit
MPH	Miles-per-hour (unit of speed/velocity)
NI myDAQ	National Instruments data acquisition device
PET-G	Polyethylene Terephthalate Glycol (3D printing material)
PLA	Polylactic Acid (3D printing material)
RW	Rear Wing
SDR	System Design Review
SJSU	San José State University
SMC	Actuator company (brand of the solenoid)
SR-13	Spartan Racing 13th Car
SRE-6	Spartan Racing Electric 6th Car
STAR-CCM+	Simcenter Computational Fluid Dynamics Software

1. Introduction

1.1 Design Backgrounds

The Drag Reduction System (DRS for short) is a commonly adapted design for Formula motor racing vehicles. The rear wing of a Formula vehicle, also known as the spoilers, is designed to produce downforce on the car to increase the grip between the tires of the car and the track. However, the existence of a rear wing creates massive air turbulence, known as drag force, when the Formula vehicle is in motion. Therefore, the drag reduction system is adapted to reduce the amount of drag force exerted on the vehicle while running down a straight racing track, which results in increased top speed and the ability to overtake (Kemble, 2022).

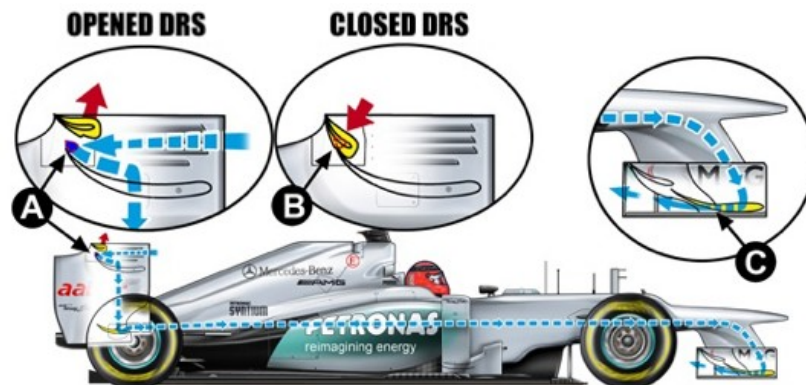


Figure 1: Typical DRS configuration on a Formula 1 vehicle

Given how complicated a Formula 1 vehicle is, the driver of the vehicle can easily get distracted by the vast amount of information displayed on the vehicle's dashboard, apart from focusing on the vehicle course while switching between different gears manually. Unless the driver is experienced in actuating the Drag Reduction System without losing the focus on the road, it is hard for the driver to make use of the DRS in real-life situations. Typically, the driver has to actuate the DRS while both hands are on the steering wheel and both eyes are on the road (Golson, 2014). Therefore, an automatic

option of the DRS is introduced to help drivers take control of the DRS while keeping the driver's on-road attention. In certain cases, Formula car drivers prefer having full control of the DRS. Thus, the manual option is preserved to accommodate drivers' preferences.



Figure 2: Steering wheel of the Sauber C33 Formula 1 vehicle

This senior project focuses on the construction and different actuation methods of the Drag Reduction System. The final prototype of the DRS can switch between two major modes: Manual and Automatic. The manual mode allows the driver to be in control of when the rear wing flaps are opened or closed. This method is perfect for experienced drivers who know when and where the DRS should be activated. The manual method gives the driver full control of the DRS. When the driver pressed the momentary button located on the steering wheel, the DRS will be activated. As soon as the driver releases the button, the DRS will be deactivated. The automatic mode, on the hand, does not give the driver control of the DRS. This method is perfect for new drivers who do not want to pay extra attention to the on-the-road condition while driving. The automatic mode will autonomously activate and deactivate the DRS. When the system recognizes that the car is on a straight track or making a turn through sensor parameters from the Inertial Measurement Unit (IMU), the wheel speed sensor, and a set of linear or angular position

sensors, the Electronic Control Unit (ECU) will send a signal to the pneumatic solenoid to open or close the pneumatic piston accordingly.

1.2 Design Objectives & Specifications

Through the implementation of a drag reduction system, the team aims to reduce the amount of drag force by varying the angle of attack (AoA) of the rear wing flaps. The project also has the objective of reducing vehicle lap times through increased straightaway speed. Ideally, the system would also reduce the amount of fuel usage, although the amount will not be significant. Through the data collected from the computational fluid dynamics study using Siemens STAR-CCM+ software (see Appendix A), the team validated that when the AoA of the rear wing increases (when the rear wing flap closes), the amount of drag force exerted on the vehicle increases as well. Alternatively, when the AoA is at 0 degrees (DRS opened), the amount of drag force decreases significantly.

The team also aims to add the ability to toggle between the manual and automatic modes. The design needs to automatically open or close the rear wing flap depending on the algorithm that attempts to gauge if there is an available grip. The team was able to program the DRS algorithm in MoTeC M1 Build to enable and disable DRS when specific sensor threshold values are met. Through the simulation of a preliminary pneumatic system prototype, the team verified that the program was capable of switching between the manual and automatic modes through a rotary encoder.

On a component level, the functional requirements, and specifications of each component are as follows:

1. Air Bottle/Tank
 - a. Adequate supply of pressurized air.

- b. The air supply can not be depleted by other car systems such as shifting.
 - c. Pressurized air storage receptacles should be isolated from one another.
 - d. 9/16” pneumatic fitting.
2. Pneumatic Solenoid/Valve
- a. Composite wings need to be modulated quickly.
 - b. Forces exerted on the dynamic wings during modulation can not push composite material past the yielding point of stress and strain.
 - c. 9/16” pneumatic fitting.
3. Pneumatic Piston
- a. Lightweight, does not increase overall vehicle weight.
 - b. 9/16” pneumatic fitting.
 - c. 2” piston travel distance.
4. Steering angle Sensor
- a. Relay angle that front wheels make with the line of symmetry of the car.
 - b. Report data to ECU quickly.
 - c. Additional sensor mounted for backup.
5. Inertial Measurement Unit (IMU)
- a. Relay car speed (velocity) to ECU program.
 - b. Provide continuous or minimal time interval discrete data.
6. Brake Pressure Sensor
- a. Withstand moderately high temperature of brake fluid
 - b. Report data back to ECU quickly.
 - c. Have a second sensor installed for backup.
7. Brake Fluid Temperature Sensor
- a. Withstand moderately high temperature of brake fluid.
 - b. Quickly report data back to ECU.
 - c. Alert driver of failing brake system performance.
8. Throttle Position Sensor

- a. Be durable to withstand vibrations and aggressive actuation of the accelerator pedal.
 - b. Report data back to ECU quickly.
9. Manual Mode Momentary Button
- a. Acts as a “fail-safe” in the event the solenoid malfunctions.
 - b. Should be easy for the driver to operate and not introduce unnecessary components to the car.

1.3 Literature Review

The Drag Reduction System is commonly used in the Formula 1 world. Its main purpose is to provide as much downforce as possible. For reference, the DRS could increase vehicle performance by 5-7 km/h (PresticeBDT, 2021). Alternatively, it can be used to overtake an opponent in a straight line moment during the race giving the advantage to pass the cars in front of them, as illustrated in Figure 3. What sets the team’s design different from a typical DRS system is the set of driver control options that the team is implementing on this project. In the manual state, drivers are given full control of the DRS system where they will be able to open and close the flaps at any time they desire. The second state will be fully automatic where the ECU will have full control of whether to activate the DRS or close the DRS. The factors affecting the state of the DRS system, in this case, are the steering angle, velocity, braking pressure, brake position, and throttle position.

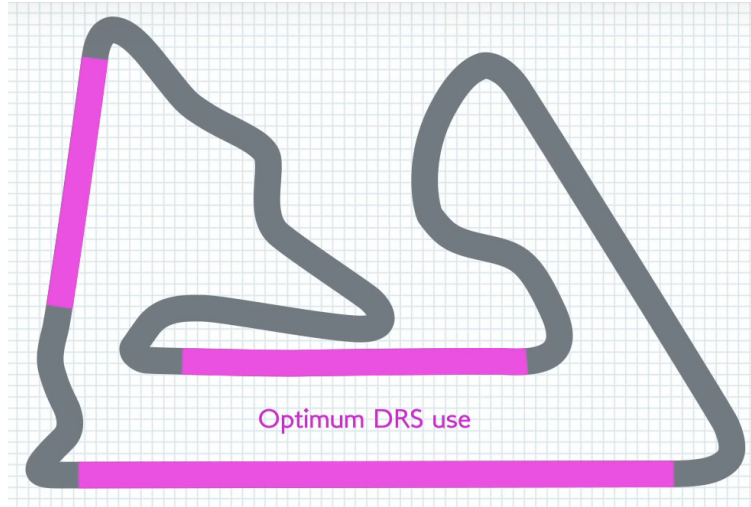


Figure 3: Track Map Example showing the Optimum ‘DRS Zone’ on Straight Paths

2. Theory

2.1 Angle of Attack and Drag Force

The angle of attack is defined as the angle between the chord line of the airfoil and the direction of the relative wind (Stoops. 2013), see Figure 4. According to Benson (n.d.), the relationship between the angle of attack and the drag coefficient is defined as

$$C_d \approx 1.28 \sin(\alpha)$$

Where C_d represents the drag coefficient and α represents the angle of attack. The drag coefficient is part of the equation to determine the amount of drag force acting on the object, which can be derived as

$$D = C_d \frac{\rho V^2}{2} A$$

Where D represents the drag force, ρ represents density, V represents velocity, and A represents the reference area. Drag force is a force, created by air resistance, that opposes an object's motion through the air. The relationship between the drag force and angle of attack can be visualized through the graph shown in Figure 5.

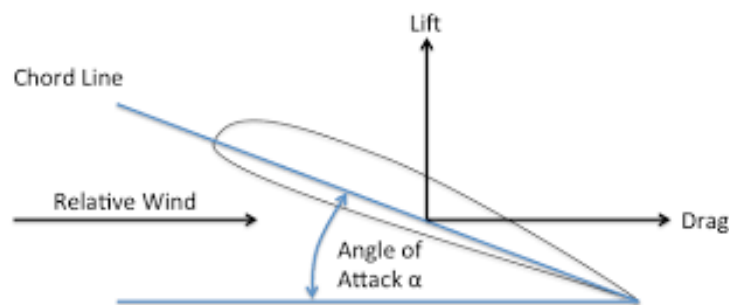


Figure 4: Illustration showing the angle of attack and directions of lift and drag force

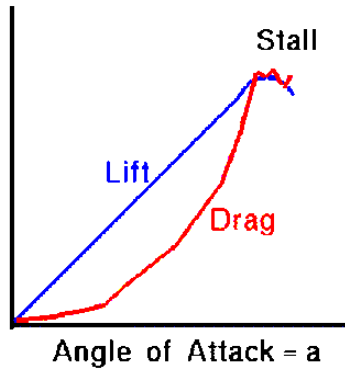


Figure 5: Graph of Angle-of-Attack against Lift and Drag force

Benson’s graph shows that the drag force will increase exponentially up to the point where the object (aircraft) stalls. A stall happens when the angle of attack of the aircraft has exceeded 20 degrees and air turbulence is created above the airfoil that would lead to a loss of the lift force. As long as the angle of attack of the airfoil is well below 20 degrees, the study concludes that the drag force will increase as the angle of attack increases. The results collected from the rear wing simulation (see Appendix A) proves that the drag force does increase as the angle of attack increases. On a side note, the concept of stall does not apply to the Drag Reduction System. The angle of attack analyzed and adopted by the DRS design does exceed 20 degrees.

2.2 Hooke’s Law

Hooke’s Law states that the displacement of spring is directly proportional to the acting force or load (Encyclopedia Britannica, n.d.). The equation of Hooke’s Law can be defined as

$$F = kx$$

Where F represents the spring force, k represents the spring constant, and x represents the displacement of the spring. The Drag Reduction Project utilizes a simple return spring mechanism to retract the piston in the case that the pneumatic system fails. After the spring constant was calculated and analyzed, a spring with the appropriate specification was selected and installed on the project.

2.3 Linear and Rotary Position Sensor

The concept of a linear or a rotary position sensor is very similar to a potentiometer. A potentiometer is essentially an adjustable variable resistor. The relationship between the resistance and the voltage of a potentiometer can be defined as

$$V_{out} = \frac{R_2}{R_1 + R_2} V_{in}$$

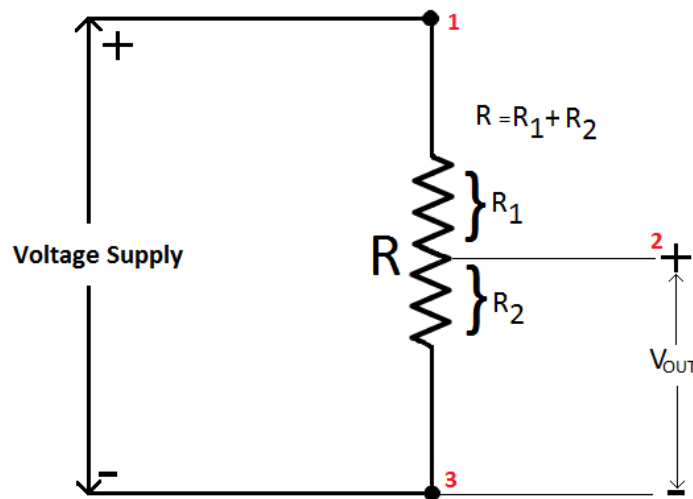


Figure 6: Schematic diagram of a potentiometer

Where V_{out} represents the output voltage, V_{in} represents the supply voltage, and $R = R_1 + R_2$ represents the rated resistance of the potentiometer.

Unlike most potentiometers, the linear and rotary position sensors do not necessarily have a rated resistance. The relationship between the output voltage and the distance traveled by the position sensors can be defined through calibrations. Generally speaking, the distance traveled by the position sensor is linearly proportional to the output voltage, in the form of

$$y = mx + c \quad \text{or} \quad V_{out} = mx + c$$

Where y represents the voltage output, m represents the gradient or multiplier, x represents the distance traveled by the position sensor, and c represents the zero distance offset of the sensor. The calibration results of one of the throttle position sensors used for the DRS can be found in Appendix B.

3. Design

3.1 Mechanical Design

3.1.1 CFD Data Analysis

Using the Simcenter STAR-CCM+ Computational Fluid Dynamics (CFD) simulation software, the aerodynamics team from Spartan Racing was able to generate a CFD simulation result of different configurations of the rear wing (spoiler). The complete results generated can be found in Appendix A, and the illustration of the simulation is shown in Figure 7. The rear wing of the Formula vehicle has a total of three possible actuating flaps. From the result, the DRS team decided that the lower two rear wing flaps are the best option to actuate the drag reduction system efficiently. Although the option to actuate all three flaps reduces more of the drag force acting on the car, it would create a center of pressure that is too high, as shown in Table 1. Similarly, although the option to actuate the top two flaps reduces more drag force compared to the option of actuating the lower two flaps, the simulation shows that actuating the top two flaps would create a 79.45% center of pressure, 5.16% higher than the option of actuating the lower two flaps.

Table 1: CFD results at a 0-degree angle of attack and 55 mph

Rear Wing Configurations	Full Car DF (lbs)	Full Car DF (N)	Rear Wing DF (lbs)	Full Car Drag (lbs)	Full Car Drag (N)	Rear Wing Drag (lbs)	CoP (%F)
Baseline	255.8	1137.86	111.56	122.6	545.35	51.1	51.7
Upper 2 Flaps Open	186.06	827.64	54.48	77.6	345.18	18.1	79.45
Lower 2 Flaps Open	192.1	854.50	59.82	79.58	353.99	23.2	74.29
All Flaps Open	164.5	731.73	38.38	68.8	306.04	12.79	89.9

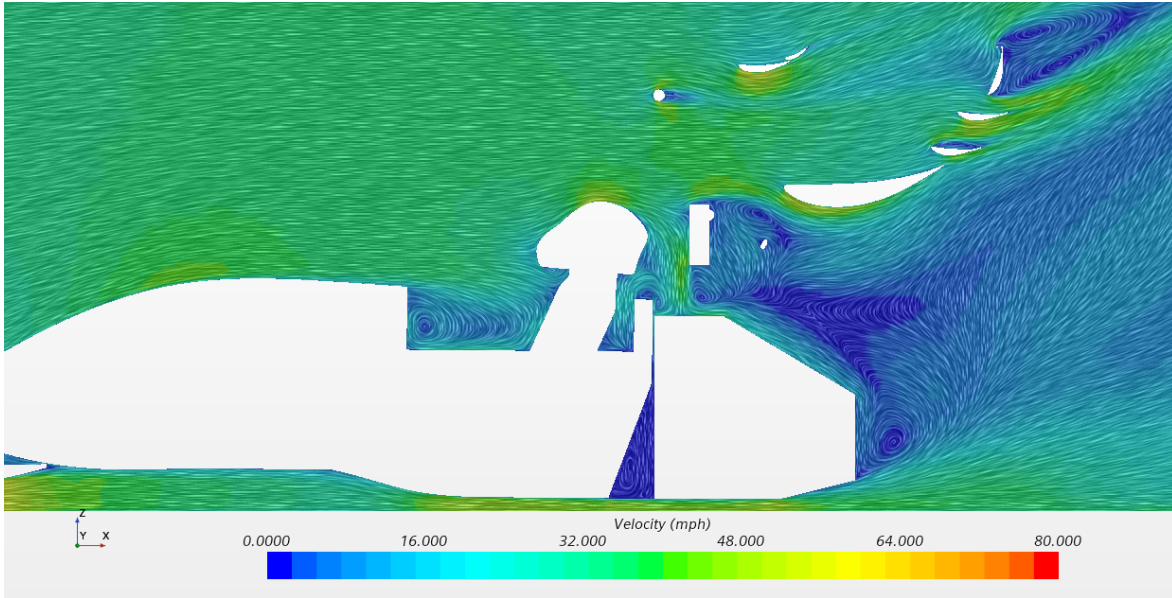


Figure 7: Computational fluid dynamics analysis of the rear wing

3.1.2 Rear Wing Foil Sleeve Design

To ensure that the mechanical linkages of the drag reduction system do not exert all of the force on the rear wing which could break the airfoils, 2 sets of foil sleeves were designed to defuse the pressure acting on the airfoils. These foil sleeves go on each side of the mechanical linkage. To create the foil sleeves according to the airfoil dimension in CAD, the team traced the actual dimensions of the rear wing airfoils on paper. Then, the image is uploaded to the SolidWorks software to be traced. Several models of the foil sleeves were printed to test their fitting on the airfoils. These foil sleeves were printed in carbon fiber nylon filaments such that it does not add additional weight to the vehicle. The foil sleeves were consecutively mounted to the mechanical linkages using pop rivets. A typical rivet has two elements; a pin and a rivet. The pin is pulled through the rivet with the pop rivet pliers, and the deformed rivet will attach the sheet metal and

3D-printed part (Ryan, 2003). The method of pop riveting is especially ideal for cases like the DRS where the materials (aluminum or plastic) are thin.



Figure 8: Foil sleeves 3D-printed using carbon fiber nylons



Figure 9: Foil sleeves assembled on the rear wing airfoils

3.1.3 Rear Wing End Caps Design

The airfoils dedicated for the Drag Reduction System are required to rotate along the axis parallel to the length of the airfoil body. A set of end caps were designed using the same method of tracing with the foil sleeves in SolidWorks. The team traced the actual dimensions of the rear wing airfoils on paper before uploading the scanned image to the SolidWorks software. The final prototypes were tested to see if it fits and the end caps with appropriate dimensions were 3D-printed using Carbon-Fiber Nylon filaments. Heat-set inserts, hardware commonly used on 3D-printed thermoplastics, were installed on the end caps such that bolts or screws can be fastened on the 3D-printed end caps.



Figure 10: End caps 3D-printed in Carbon-Fiber Nylon



Figure 11: Bonded end caps on the side of the DRS airfoils

3.1.4 Mechanical Linkage Design

The main requirement of our project was to have the ability to control and transition rear wing flaps between two positions. With this as the functional requirement, many different mechanisms were considered. Three types of mechanisms entered the final selection. The three were pulley type transmission, individual servo motor drive, and mechanical linkage mechanism. The mechanism selection is finalized alongside actuator selection with similar considerations such as packaging, manufacturability, cost,

weight, speed, repeatability, and effect on the aerodynamic characteristics of the rear wing.

The mechanism selected is a linear pneumatic piston actuated four-bar linkage mechanism. There are many advantages of this mechanism over the others that were considered. The four-bar linkage mechanism has a small footprint in the confines of the rear wing which reduces the impact on the overall aerodynamic performance. The decision to use mostly sheet metal construction reduces manufacturing costs and time. A semi-rigid mechanism would result in less deflection and more direct transmission of force. With the moving components being lightweight and the power of the pneumatic piston, the mechanism is capable of extremely low cycle time. The downsides of the linear pneumatic piston actuated four-bar linkage mechanism was determined to be a worthy compromise. One of the disadvantages of this mechanism is its overall weight and bulk. With all of the components combined, the weight of the entire system is easily triple the lightest option, the individual servo motor drive, though the center of gravity would be lower.

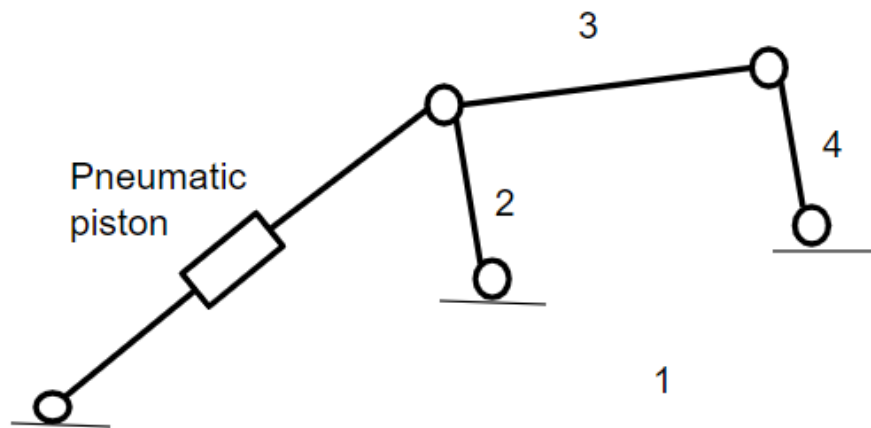


Figure 12: linear pneumatic piston actuated four-bar linkage mechanism diagram.

3.1.5 4-bar Linkage design

The main mechanism of the DRS system is a pneumatic piston actuated 4-bar linkage. The mechanism is constrained in two-dimensional movement by the ground link which is the rear wing structure. The purpose of this mechanism is to rotate and position the middle two flaps on the rear wing assembly between the designed Angle of attack (AoA) and flat, lowest drag position.

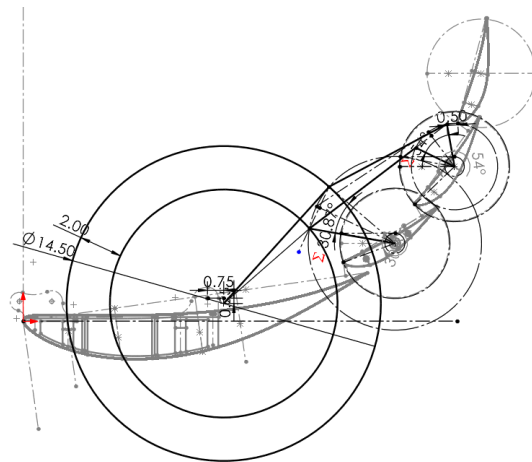


Figure 13: SolidWorks CAD of Mechanism Kinematic Sketch

The main design factors that were considered during the designing of this mechanism are packaging, component compatibility, and efficiency. In terms of packaging, the areas of focus are the proximity of the linkage nodes in relation to the other components and wing elements to prevent collision during operation; the frontal area of different components, and the aero profile change of the flaps incurred by the mounted components. Component compatibility between all the parts and other potential options of off-the-shelf components were considered in case of the difficulty sourcing specific components now or in the future. A major interest and potential gain from the design of the kinematic is the mechanical efficiency of the mechanism. A high mechanical efficiency would reduce the weight of most components, lessen the loads on the composite flaps, and increase the number of available actuations with the same

amount of air in the air tank. The method to evaluate the mechanical efficiency of a four-bar mechanism is through the transmission angle value. A high transmission angle entails a high mechanical efficiency of the mechanism. The analytical definition of transmission angle is:

$$\tan \mu = \frac{\text{Force component tending to move the driven link}}{\text{Force component tending to apply pressure on driven link bearings}} \quad (3)$$

$$\sin \mu = \frac{\text{Force component tending to move the driven link}}{\text{Total force applied to the driven link}} \quad (4)$$

The graphical definition of transmission angle is the angle formed by the force transmitting member to the driven member. The two transmission angles in this 4 bar mechanism are 50.9 degrees and 63.8 degrees respectively shown in the figures.

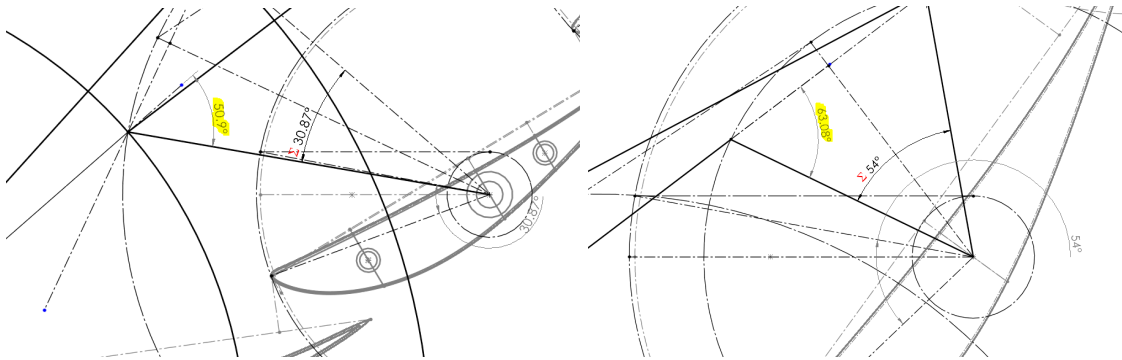


Figure 14: SolidWorks CAD Demonstration of the Transmission Angles

Using the sketch, by varying the different total lengths of the actuator bolt to bolt distance a set of transmission angles was calculated. Using the calculated transmission angle, three configurations with different efficiency characteristics stood out. The three configurations are best overall average efficiency, best downstroke efficiency, and best upstroke efficiency. The three outstanding geometry configurations have a total length of 6in, 6.75in, and 7.25in.

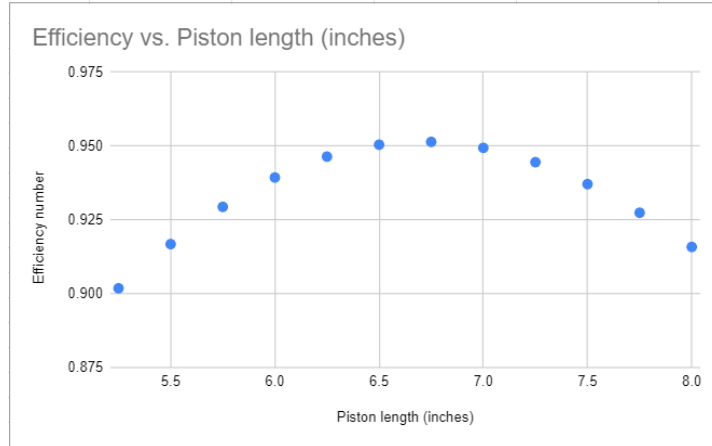


Figure 15: Efficiency vs. Actuator total length graph

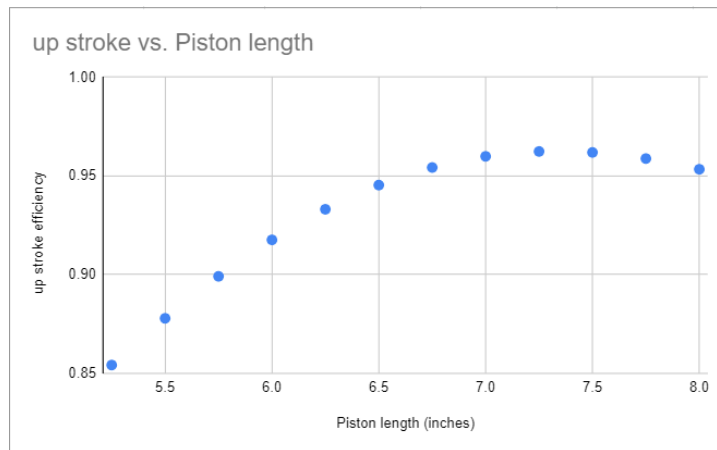


Figure 16: Upstroke efficiency vs. Actuator total length graph

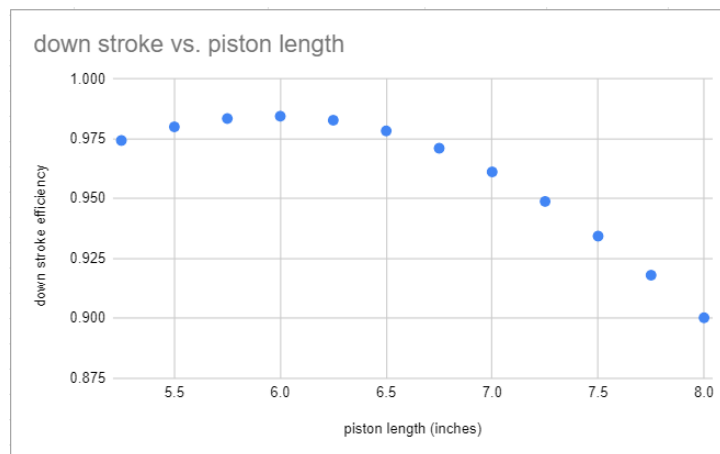


Figure 17: Downstroke efficiency vs. Actuator total length graph

3.1.6 Rear Wing Mounting

As part of the four-bar linkage and the main rear wing interfacing component, the rear wing foil mounting was an important part of the design. The goals and requirements of the foil mounts are low cost, lightweight, close fit to the handmade airfoils, and maintain position during actuation. To achieve these goals the foil mount was designed to be a three-piece construction with a sheet metal centerpiece and two 3D-printed sleeves sandwiched beside. This design was chosen because it cost the least, fast manufacturing turnaround time, and is lightweight. Using a traced sketch of the airfoil profile, the sheet metal part was drawn up with a 0.01-inch mating gap to ensure close-fitting. The bolt location was determined by the previously mentioned four-bar mechanism geometry. The sleeves are secured to the sheet metal part using rivets. To connect the two foil mounts, a pair of dog bone shape sheet metal links were used. The sheet metal parts are jointed using #10 hardware. The material chosen for the sheet metal components is aluminum 6061-t6 alloy because of cost and weight.

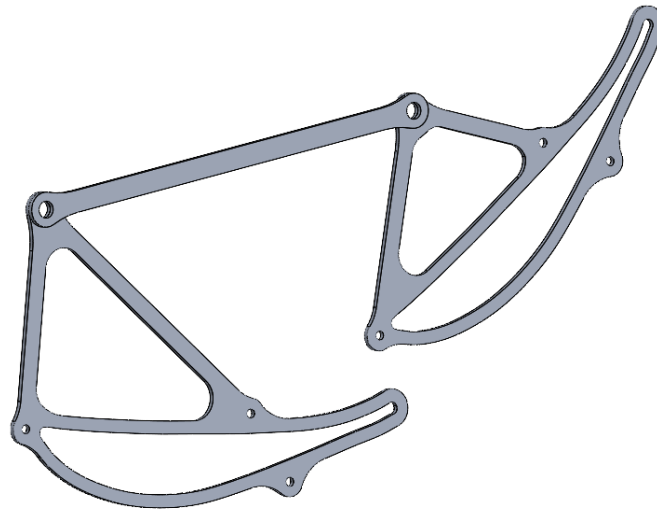


Figure 18: Sheet metal rear wing foil mount shown in CAD



Figure 19: Sheet metal rear wing foil mount test fit on rear wing foil

3.1.7 Piston Clevis Design

The component that allows us to vary the four-bar linkage mechanism geometry is the length of the piston clevis. By changing the length of this part, the total length of the pneumatic piston assembly can be varied.

The piston clevis end condition is, on one side, 10-32 thread stud on the piston end and, on the other end, sheet metal part of the four-bar mechanism. The material used is the aluminum 6061-t6 alloy for cost and ease of machining. The part is subjected to the full force of the pneumatic piston under working conditions. The force is expected to be 30lbf. This part was designed with manufacturability in mind and ease of machining. The part was analyzed using Solidworks finite element analysis for the factor of safety and buckling.

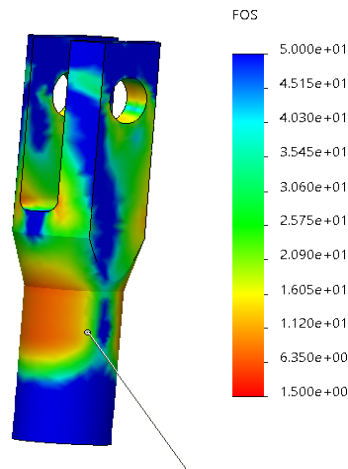


Figure 20: Solidworks finite element analysis factor of safety plot

Model name: 13-FR-60009-1A-Piston_end_clevis
 Study name: Buckling 1(-Default-)
 Plot type: Buckling Amplitude1
 Mode Shape : 1 Load Factor = 79.191
 Deformation scale: 0.383565

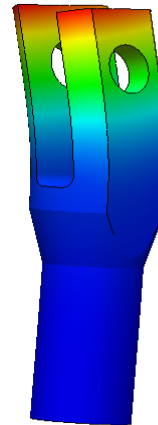


Figure 21: Solidworks finite element analysis buckling plot

3.1.8 Air Bottle Mounting

The air bottle of the Drag Reduction System is mounted differently on the combustion (SR-13) and the electric (SRE-6) car manufactured by the Spartan Racing, SJSU Formula SAE team. This is because, in the combustion car, a second air bottle is

used for the gear shifting mechanism, while the electric car does not need an air bottle for the shifting mechanism. Therefore, it makes more sense to mount the two shifting bottles on the combustion car together. On the combustion car, the air bottles are mounted on a 3D-printed mount and fastened to the top of the engine, as shown in Figure 23. The air bottle holder was designed with a hose clamp fitting to tie up the air bottles securely. The air bottle holder was 3D-printed using Polyethylene Terephthalate Glycol filaments.

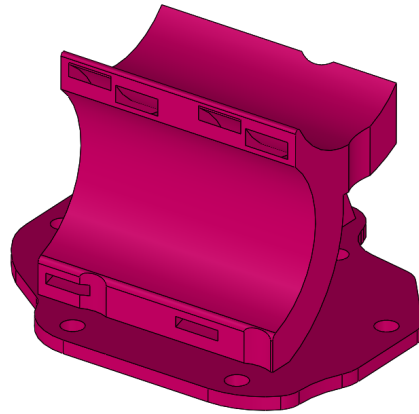


Figure 22: Air bottle mount SolidWorks part model with hose clamp fitting

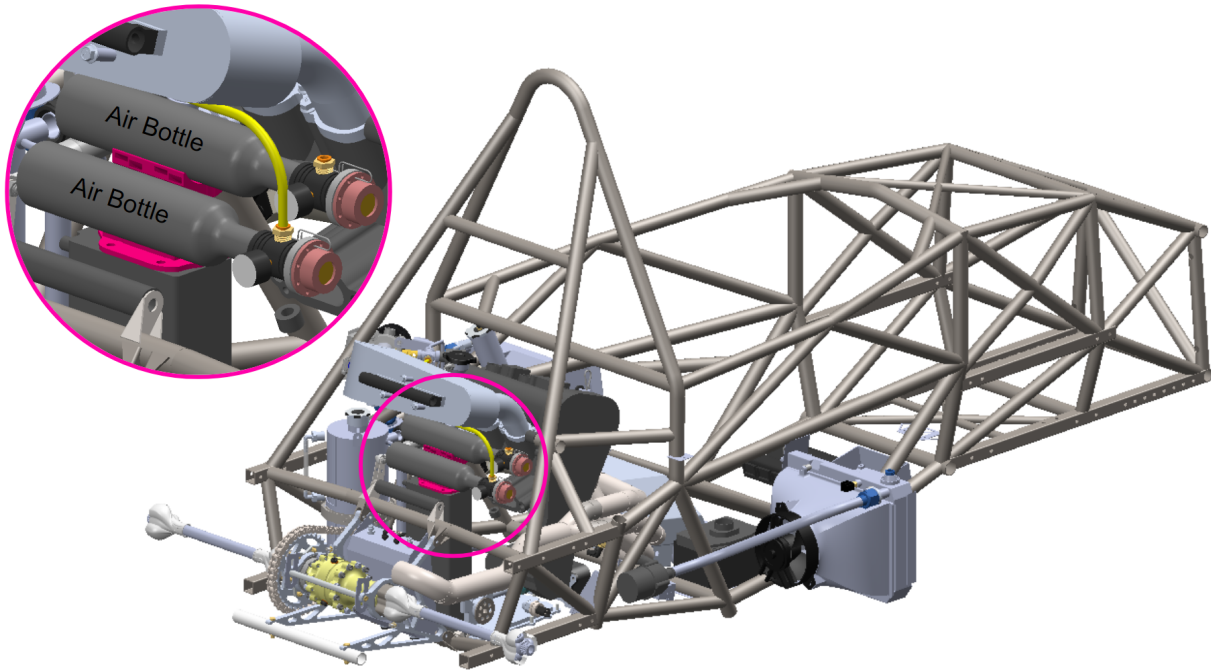


Figure 23: Air bottle mount (highlighted in pink) location on the combustion car

As for the electric car, the air bottle used on the DRS is mounted on the roll hoop bar of the electric car, as shown in Figure 24. Unlike the combustion car, the electric car does not have an internal combustion engine, so the mounting point of the air bottles needs to be shifted. The air bottle mount designed for the electric car consists of a sheet metal bracket, air bottle holder, and a set of hose clamps. The sheet metal bracket was designed with multiple cut-outs in the middle to minimize the use of materials and to reduce the overall weight of the bracket acting on the car. The sheet metal bracket was ordered through an online laser and CNC cutting service, and the material selected was 4130 Steel. The bracket was welded on the electric car's roll hoop bar.

The air bottle holder was 3D-printed using Polyethylene Terephthalate Glycol (PET-G) filaments. The design contains a set of hose clamp fitting and hole clearance for 6-32 screws. One of the air bottle holders was designed with a “bottleneck holder” to

support the air bottle and prevent it from sliding down the mount. The air bottle was also designed to be mounted facing away from the driver's torso so that in cases of emergency, the driver's head and torso are not in the hazardous range. The assembly of the air bottle mounts made for the electric car can be seen in Figure 25.

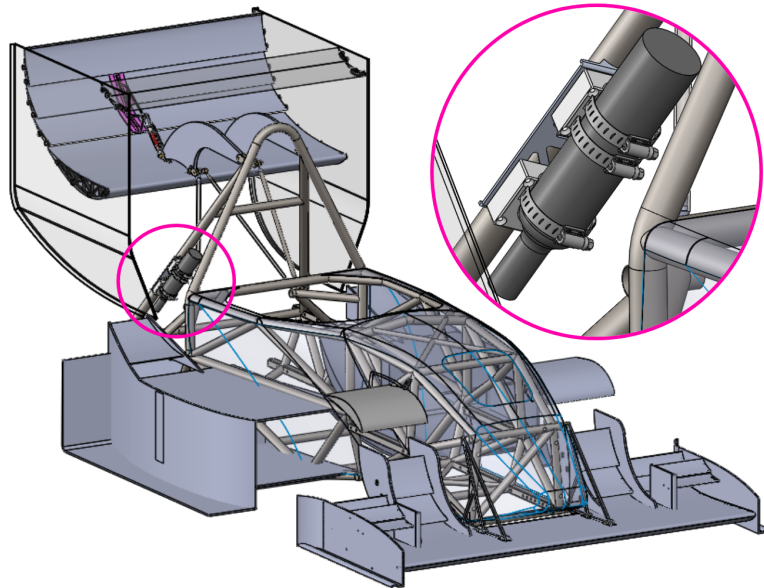


Figure 24: Air bottle mount (highlighted in pink) location on the electric car

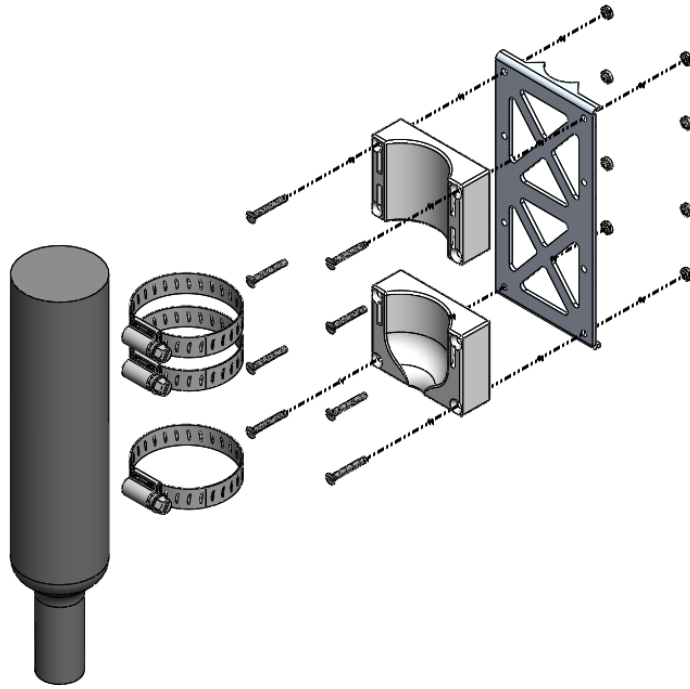


Figure 25: Air bottle mount assembly exploded view

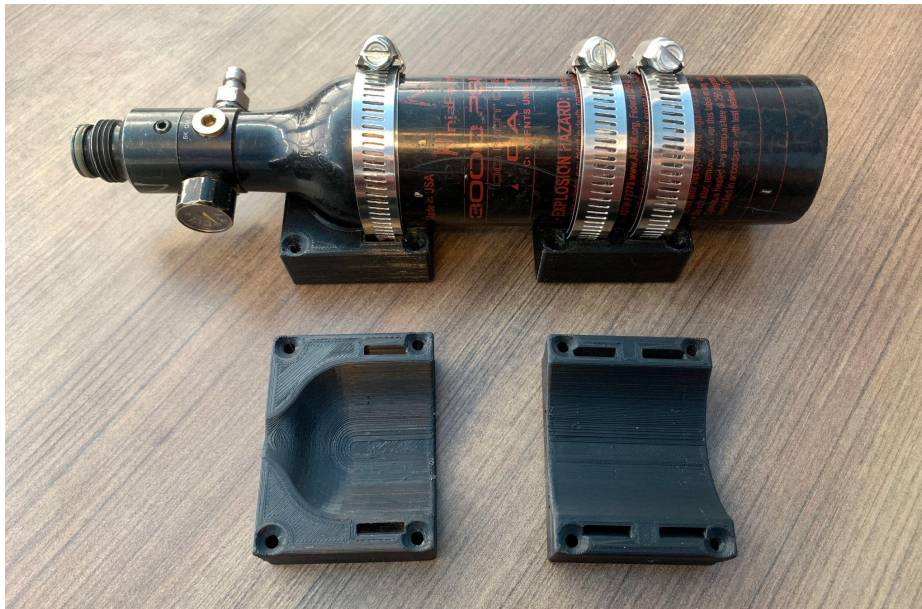


Figure 26: Air bottle mount with air bottle secured

3.1.9 Return Spring Design

A return spring design was incorporated to act as a failsafe of the pneumatic system such that in the cases of emergency when the pneumatic system fails, the spring will be able to retract the pneumatic piston's end back to its original (closed) position. Throughout the development of a return spring mechanism, there have been endless discussions about whether the implementation of a return spring was necessary. That is because when the car is running at high speed, the amount of air pressure acting on the vehicle's rear wing would close up the rear wing flaps and thus bring the piston back to its original position. Nevertheless, the team concluded that a return spring is not a must-have but still a good-to-have failsafe mechanism for the pneumatic system.

The first proposed design for the return spring mechanism, shown in Figure 27, consists of a pair of shaft collars, a pair of sheet metal spacers, and an extension spring. The shaft collars are essentially a pair of clamps that are fastened with hex cap bolts. The shaft collars will clamp onto the body of the piston on one end, and the body of the piston, clevis on the other. A pair of sheet metal spacers will hold the spring in place and parallel to the body of the piston such that the spring does not rub against the pneumatic components during actuations. However, it was later determined that the implementation of shaft collars is not feasible since they could slip away from the body of the piston or clevis and it adds complexity to the mechanism.

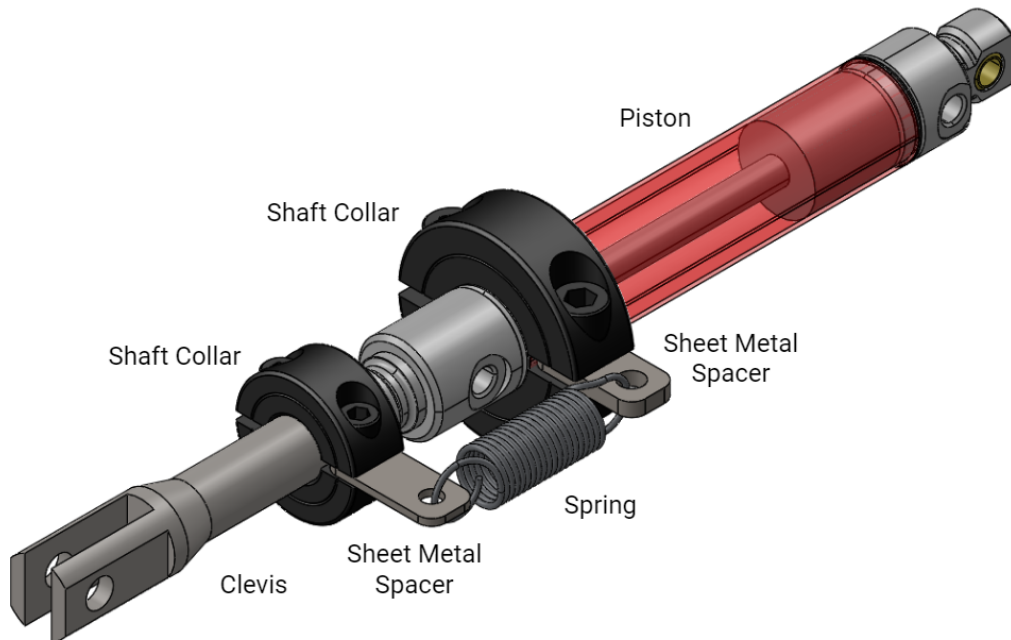


Figure 27: Proposed return spring design (first version)

Therefore, the team decided to come up with a revised return spring mechanism that would eliminate the use of the shaft collars. The design, shown in Figure 28, consists of just a pair of sheet metal mounts and an extension spring. The updated design also reduces the cost of production. The new design utilizes the sheet metals as both a spring holder and mount on the pneumatic piston. One of the brackets is fastened to the piston's lower end while the other is fastened to the piston's clevis. As for the spring, it was determined through calculations (see Appendix B) that any spring that is rated with a spring constant greater than 2.44 lbf/in is appropriate for the mechanism. The team also established that since the presence of a return spring is not significant in the drag reduction system, the selected spring does not require to be on specification, as long as the spring has enough stiffness to not break during actuations.

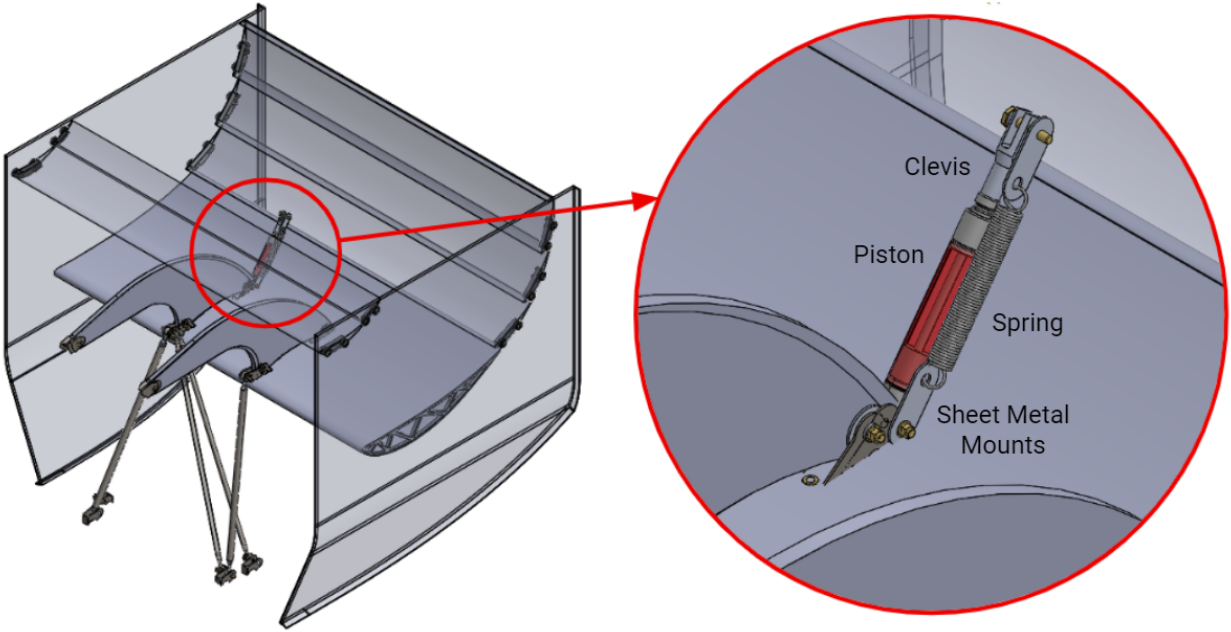


Figure 28: Revised return spring design (second version)

3.2 Controls Design

3.2.1 Sensor Data Analysis

Research and development for the automation algorithm consisted of reviewing available sensors on the vehicle and determining the quality of their outputs. Several components are used to interpret and record data such as the ECU, DAQ, and IMU. Data is transmitted over CAN, serial, and analog buses. MoTeC manufactures the ECU and DAQ while Aceinna makes the IMU. MoTeC software M1 Build, M1 Tune, and i2 Pro were used to analyze recorded sensor data from the previous endurance racing event of 2021 in Michigan. Before the algorithm was tested, considerable time was spent reviewing the race data so that program speculations could be more accurate.

The i2 Pro software displays recorded race data for a selected time interval, as shown in Figure 29. An additional feature of the program is that it utilizes GPS and satellite information to overlay the path of motion that the car traveled at a particular time and show the corresponding data values. With data graphically displayed, it was easier to determine which sensors appeared to have more noise, such as steering rate. For baseline functionality, throttle pedal position and steering angle was defined as the bare minimum parameters of the algorithm. Using the track image overlay feature, data was analyzed at moments when the car was known to be traveling through a straight section. At these straights, the initial threshold values for selected parameters could be determined by reviewing sensor outputs, sensor noise, and car behavior.



Figure 29: I2 Pro Data Analysis from Michigan with Track Overlay

3.2.2 Sensor Selection

For the initial prototype of DRS, data was retrieved from the ECU as it hosted the previously defined bare minimum parameters, throttle pedal position, and steering angle. The throttle pedal position was selected over the intake manifold throttle blade position as the ECU can control the throttle blade independently of the pedal position and driver inputs. With the goal of DRS actuating on straight sections of track, steering became the second parameter of choice. By reducing the size of the steering angle threshold, DRS actuations could be prevented from happening in turns while the driver had the steering wheel held to either side. Additional parameters were brake pressure, vehicle velocity, and slip ratio. Brake pressure was analyzed from the front wheels, where the majority of braking force is applied to the car. In braking situations, the driver would benefit from increased drag and downforce, and to enhance safety in these scenarios, brake pressure would be one of the triggers to close the DRS. Vehicle speed is obtained from the wheel speed sensors and can be referenced from an onboard accelerometer. The DRS has

negligible aerodynamic benefits below 30mph and setting this velocity threshold preserves compressed air and allows for more favorable DRS actuations. Slip ratio is a calculated parameter that comes from the wheel speed sensors and can help predict when the vehicle may slip or slide on the track, potentially causing an accident. The threshold for slip ratio has been set low, about 0.2 and with on-track testing, performance will be evaluated to further optimize DRS and increase parameter thresholds.

3.2.3 Actuation Methods Analysis

In considering the type of actuator to utilize, mass, size, response time, mounting complexity, energy source, and reliability were evaluated. The rear wing of the race car is placed considerably high on the vehicle and shifts the center of gravity upward and backward. To mitigate the impact of a raised center of gravity, emphasis was placed on specifying an efficient actuator that had little mass. Research began by analyzing the different characteristics of hydraulic, linear, and rotary actuators as well as electronic or pneumatic, as seen in Table 2. The table shows the decision matrix for different kinds of actuators with their assigned score per category, with an added score multiplier for more critical attributes, such as the weight of the actuator. The highest scoring actuators were found to be pneumatic for their quick actuation speeds, compatibility with the fail-safe design, and low weight. Ultimately, the pneumatic linear actuator was selected as it scored the highest on the decision matrix which is in part due to its less obstructive aerodynamic nature when compared to the pneumatic rotary. Additionally, the pneumatic rotary would have to be installed on the rear wing, on an endplate, where torque would be applied to the dynamic airfoils from one end, increasing the chances of bending to occur. In comparison, the linear pneumatic actuator can be mounted closer to the center of the airfoils on the rear wing, reducing any induced bending by at least half through more symmetrical loading.

Table 2: Actuator Decision Matrix with Scores per Category

actuation types	system cost	additional energy source required?	actuation time	system weight	CG position (x,y,z) inches	effect on aero (10 = little interference)	durability (1 = weak)	"fail-safe" capable system (1 = no)	design time (10 is efficient)	total
Category weight (multiplier)	5	3	10	10	0	8	8	10	7	
hydraulic	5 ~	~	~	1 ~	~	5	8	9	1 ~	
stepper motors	8	10	5	3	1	5	5	1	5	275
Screw type linear actuator	10	10	1	2	1	5	8	1	10	294
servo	1	10	8	10	5	7	8	3	1	372
manual trigger, pneumatic linear	8	1	10		10	7	9	1	10	351
pneumatic, linear	5	1	10	8	10	7	10	10	9	507
pneumatic, rotary	8	1	10	7	7	6	7	10	5	452

3.2.4 Actuator Selection

Many actuation methods exist ranging from hydraulic, electric, and pneumatic. There are many possibilities to energize the DRS system on the Formula SAE car. After extensive research and decision matrix, the team narrowed it down to pneumatic or stepper motors. After comparing the pneumatic and stepper motors side to side, it was determined that the pneumatic system is the best actuation method. Many factors were considered between the two actuation methods such as weight, force, speed, and voltage draw. Although a comparison analysis was run between the actuating methods, the team concluded that the best choice was the pneumatic system as there are rules, requirements,

and specs to be considered when choosing the best fit for actuating the DRS system. While looking closely at stepper motors and pneumatics the team thought about how the actuations will benefit the team and uphold the SAE standards thus, pneumatic was the best choice.

Stepper motors are known to be notoriously expensive and heavy and would need a full redesign and a new ECU integration with the SR-13 and the SR-6 thus, leading to making it a bit more difficult to implement on the Formula SAE car and would be challenging to uphold our standards within our time frame. However, Pneumatic was the choice that made more sense considering the goals and requirements that the team is trying to achieve. The DRS system will be implemented on both electrical & combustion cars thus, the team wanted to avoid a heavy voltage draw to make it work in both cars so the team wouldn't have to design two different actuation methods. The pneumatic system is a simple actuating method where its components are an air tank, lines, valve, solenoid, and a piston; where the air pressure can be controlled and released by the solenoid in a short time allowing the DRS to be activated and deactivated within 80 milliseconds per actuation. A pneumatic system would allow the team the option to implement a return spring mechanism in case things were to go wrong on the track. The pneumatic system fits the team's goals and requirements to achieve great results and wouldn't be more than 800g of extra weight added to the car. The actuator selected for the DRS project was the BIMBA 022-DXP Pneumatic Piston shown in Figure 30.



Figure 30: BIMBA 022-DXP Pneumatic Piston

3.2.5 Pneumatic System Design

The Pneumatic System design is composed of 5 different parts that connect. First, the main component that makes the accusation possible is a double solenoid exhaust center valve that operates off a 12V system. The valve can withstand a system pressure of 120 psi and up to 145 psi maximum. It has a low power consumption of 0.65 W, and the valve supplied by SMC as it is a fast-acting valve with a response rate of 33ms. Initially, The valve has a closed center valve that was specified for the system but was found to be alarming in case of an event of valve failure. If the valve failed the piston would stay pressurized and possibly stay in the open position.

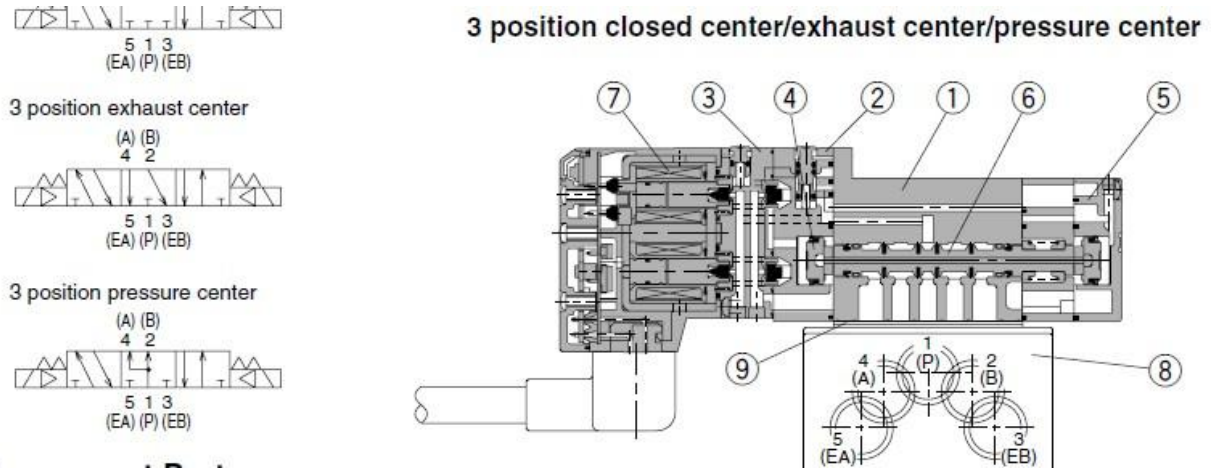


Figure 31: SMC 5 Port Solenoid Valve

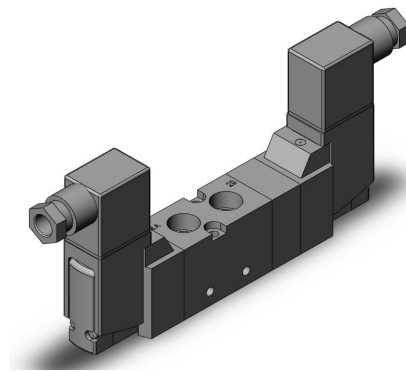


Figure 32: SMC 5 Port Solenoid Valve CAD part

There are a total of three ¼ inch lines connecting to the solenoid valve where one line goes to the air bottle and another two lines that connect from the valve to the piston where one line extends the piston and another line retracts the piston and returns to the closed position. For the air bottle, we are just using a standard 13 ci 3000 psi air soft bottle where the bottle is pressurized to 3000 psi with an output of 80 psi that goes to the solenoid valve for our application. We decided to go with a BIMBA piston 022-DXP that extends out about 2 inches from the closed position with internal bump stops that soften the return from the open position to minimize the force and vibration to not damage the

carbon fiber wing parts where the mounting points are. The last thing that makes the system operational is a 12V power source connected from two sides of the solenoid valve where one side sets the piston to the open state and the other side sets the piston to the close state. While these wires are connected to the wiring harness from the ECU that sends signals to the solenoid to open or close the piston by a button on the driver's steering wheel.

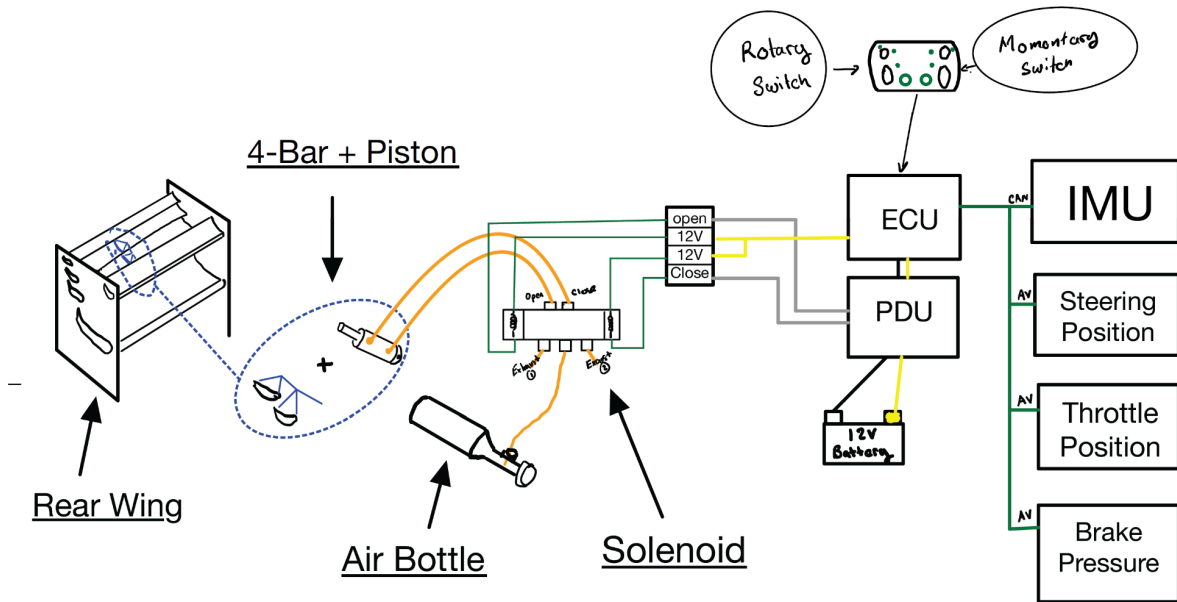


Figure 33: System Overview

3.2.6 Circuit Wiring & Control Diagrams

The circuit begins at the battery where a potential of 12V is stored. The Power Distribution Unit or PDU then distributes 12 volts to all units. Included in the aforementioned units are the ECU, IMU, and Solenoid. Given the power, the ECU supplies the PDU with a regulated 5V rail which powers the rest of the sensors including Steering Position, Throttle Position, and the Brake Pressure. These sensors feed information to the ECU over analog inputs and the CAN bus. Depending on the mode selected by the driver on the steering wheel a different state will be entered. Depending on the state, the ECU will sink current through a Half-Bridge output routed through the solenoid engaging either side. The electronic control also allows for more efficient use of power shown in Figure 34. In a situation where a 5 position relay is used to open and close the solenoid, power is used at all times. With the electronic system, power can be completely removed when the system is not in use increasing the efficiency by 95%.

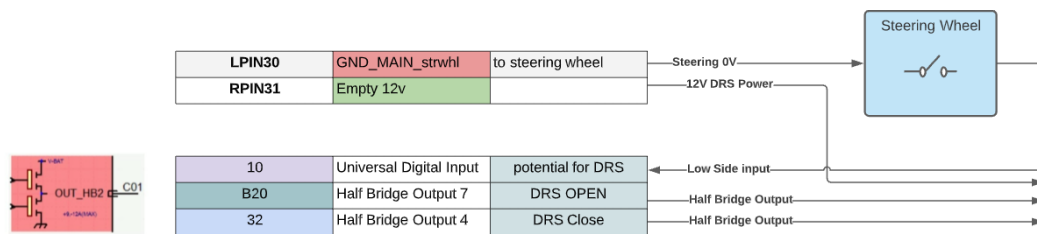


Figure 34: System Overview

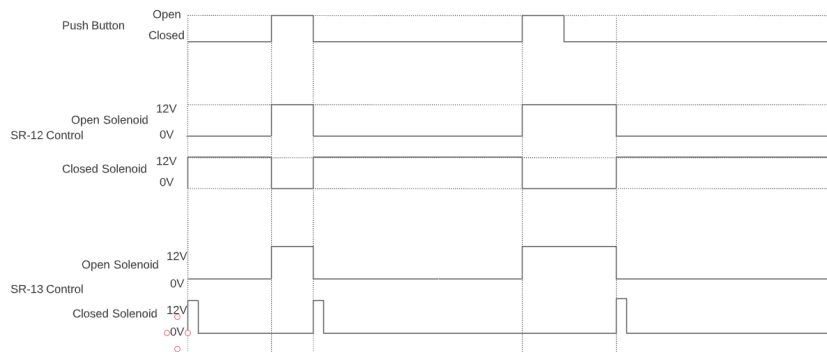


Figure 35: Open & close graph

Motorsport grade standards were kept when manufacturing the harness. Deutsch DTM Series connectors are used through the harness for their IP68 rating as well as their current and wire gauge ratings. Through the harness, we use a mix of 20 and 22 AWG wire (not including battery terminals). Since none of the systems involving DRS need high amounts of current we utilize 22 AWG for the entire system. The color code for the system is yellow for 12V, black for ground, white for signal, red for 5V, and gray for 5V ground. Each wire has a heat-shrink label applied to the end of each wire for labeling purposes.

3.2.7 MoTec Software Programming

The DRS system is controlled by the ECU which has two interfaces. The first is the M1 Tune, Tune is like a GUI allowing users to quickly change and update the parameters shown in (see Figure 54 in Appendix C) these parameters include the thresholds of each of the sensors as well hysteresis values that can be used to better tune the system and omit any unfavorable actuations. The second interface is M1 Build, here is where we set up all of the background code. M1 Build is most relatable to C++ or C#. The program allows you to set up objects with specific attributes which can be used in scheduled functions. These functions range from calculating hysteresis to calculating the current state of DRS.

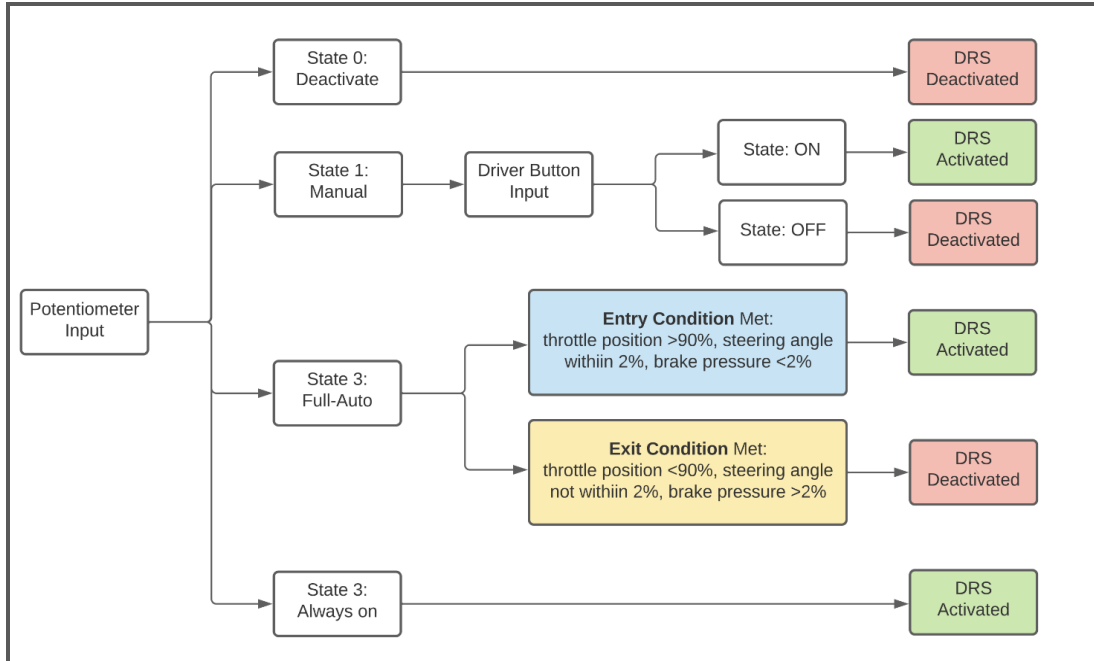


Figure 36: Block Diagram

3.3 Manufacturing and Assembly

3.3.1 Parts Manufacturing

The mechanical parts of the Drag Reduction System consist of the set of linkage, airfoil sleeves, airfoil end caps, piston mounting bracket, return spring bracket, piston end clevis, air bottle holder, and air bottle mount. Some of these parts were manufactured in-house, while some were sent out as an order to be manufactured by a service provider. The sheet metal parts, in this case, the linkages, brackets, and mounts were manufactured through SendCutSend, an online laser and CNC cutting service provider. The thickness for all sheet metal parts was set to be 0.05 inches. On some of the sheet metal parts, hole cutouts were made to minimize the material usage and also to reduce cost. The mechanical linkages were made of 6061 Aluminum alloy, an aluminum alloy that is corrosion-resistant and relatively low-cost (Huang, 2021). The main reason that 6061

Aluminum was chosen for the mechanical linkage was that it is non-corrosive so it will not rust over time. As for the brackets and mounts, 4130 Steel alloy was chosen as the material because it is a weldable material (Huang, 2021). The air bottle mounting bracket, for example, will be mounted on the vehicle's roll hoop bar.

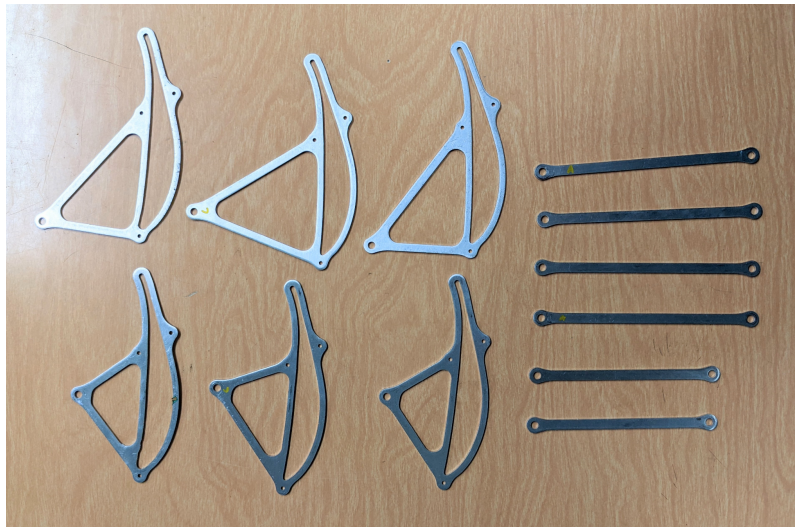


Figure 37: Sheet metal order of the mechanical linkages

The airfoil sleeves and end caps, on the other hand, were printed using 3D printers. The material involved was carbon-fiber nylon. The team managed to print the final model of the foil sleeves and end caps after test-fitting its dimension on the actual airfoils. For some 3D printers, it took several tries before a satisfactory part was printed. As for the bottle holder, the printing filament used was PET-G, which has a higher thermal resistance than PLA plastic filaments. For the piston end clevis, it was machined using the lathe and milling machine available on campus.

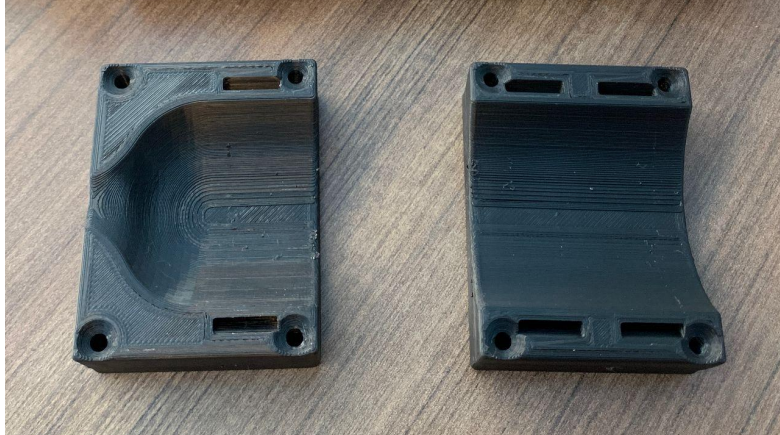


Figure 38: Air bottle holder printed with PET-G plastic filaments



Figure 39: Machined clevis using a lathe

3.3.2 Component Assembly

The first step of assembling the drag reduction system is to assemble the rear wing (spoiler) of the vehicle. The rear wing components such as the airfoils, main element, endplates, and swan necks were borrowed from the Spartan Racing, SJSU Formula SAE team's aerodynamics team. First, the foil sleeve was slid into the airfoil. Since these foil

sleeves were designed to be tight-fit, it took some effort to install them onto the airfoils. Then, the mechanical linkage was installed onto the airfoil, followed by the right foil sleeve. The three-part DRS component was adjusted to align with the right swan neck location on the rear wing (see Figure 42). The steps were repeated for the second DRS airfoil before the entire rear wing was brought together to be fastened.

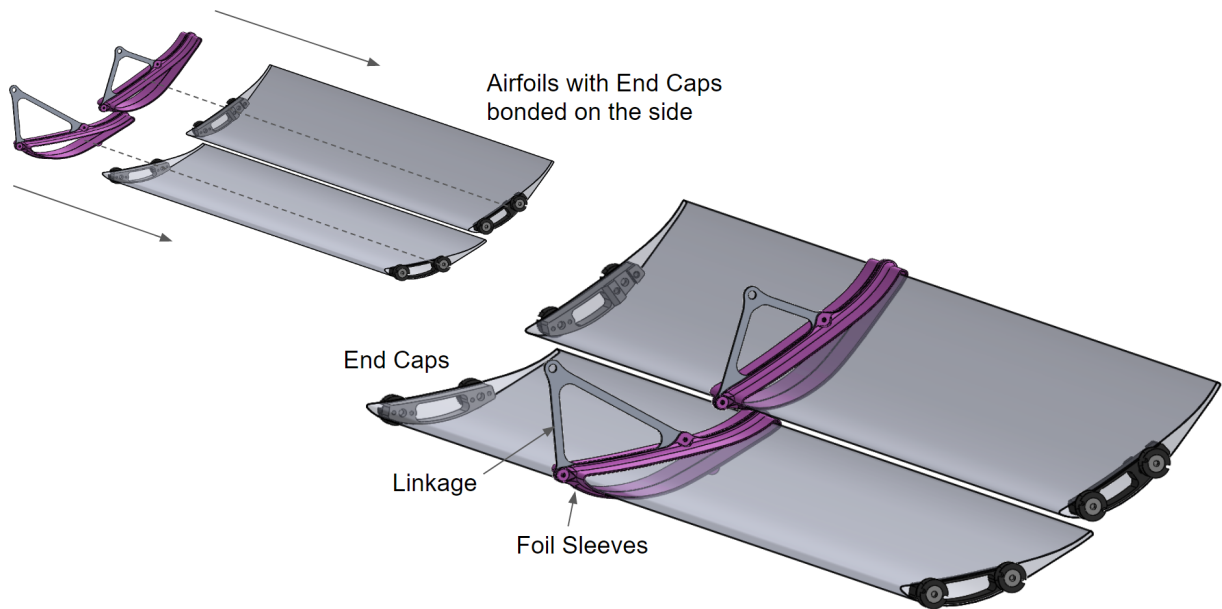


Figure 40: Installing the foil sleeves and linkage on the airfoils

Once the two actuating airfoils had the foil sleeves and linkages installed, the rest of the rear wing airfoils, including the main element, were brought together and fastened onto the endplates with sets of screws and washers. The washers were used to keep the screw from loosening up since the DRS system tends to vibrate aggressively. It is also part of the Formula SAE rules that any aerodynamic device of the vehicle (including the rear wing) has enough rigidity such that the vehicle's vibration will not damage any of the aerodynamics devices (SAE International, 2021). After the entire rear wing was brought together, the main element brackets were fastened onto the body of the main element. This bracket will serve as a mounting point for the swan necks, the DRS return spring, and the DRS pneumatic piston.

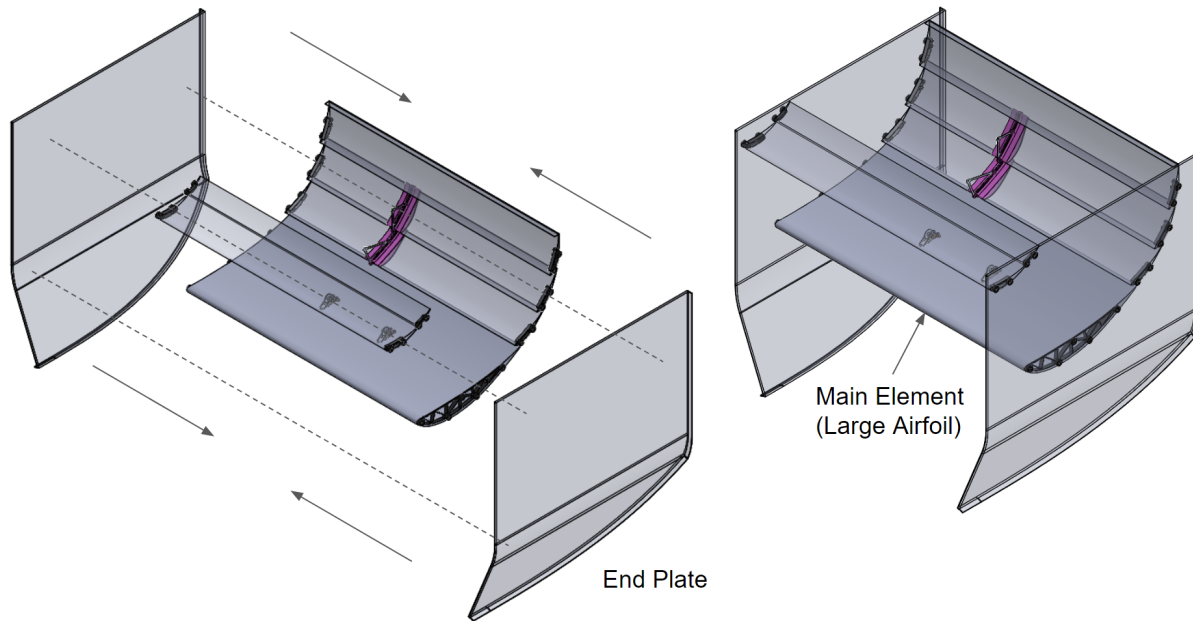


Figure 41: Installing the main element and end plate on the sides

Once the main element bracket was fastened to the rear wing, the pneumatic piston and the sheet metal bracket dedicated to the return spring were mounted through the bracket using a set of bolts and nuts. On the other end of the piston, a machined clevis was fastened onto the piston rod's end together with the DRS mechanical linkages. The complete setup of the rear wing is illustrated in Figure 42.

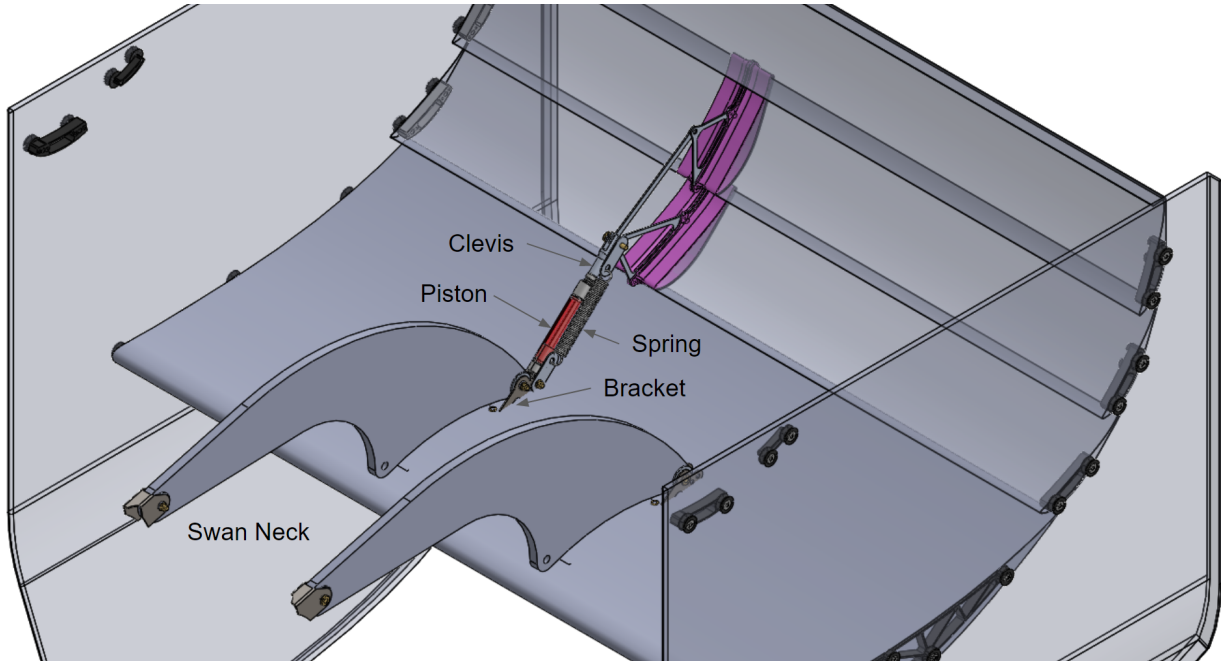


Figure 42: Installing the pneumatic piston and the return spring



Figure 43: Real-life assembly of the rear wing with DRS attached

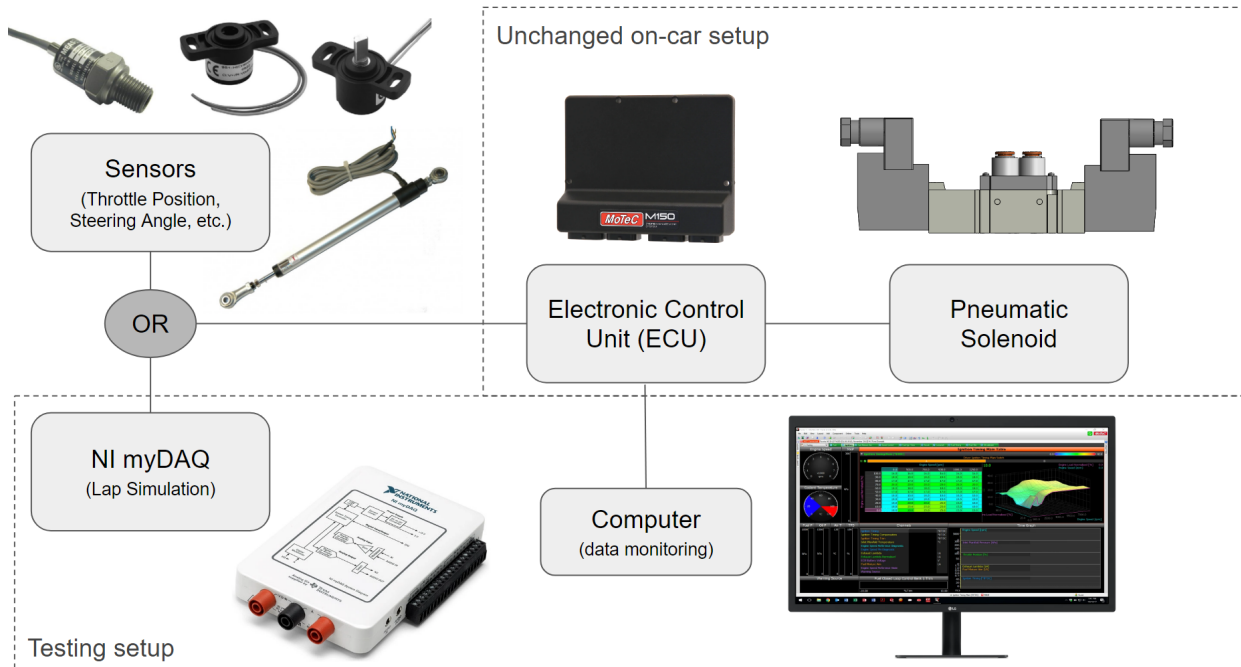


Figure 45: Electrical system connection and setup

3.4 Cost Analysis

The sponsors helped provide the team with almost all the parts needed to build this project. Thus, the sponsor helped the team keep the cost down and a much appreciated thank you to Spartan Racing Formula SAE for allowing the team to use the club's resources and tools to build this project. The aerodynamic parts were built by the Aerodynamic team which helped with the production of the wing. Overall this project cost around \$766.09 if everything was bought with pocket money, but the sponsors were kind enough to support the team in building and supplying all the necessary parts to put this project together.

Table 3: Bill of Material (BoM)

Item #	Serial # / part #	Item Name	Source	QTY	Cost (each)
1	Bimba 022-DXPB	9/16" x 2" Double Acting Piston	BIMBA	2	50.60
2	SMC TIA07B-33 tube, nylon, 1/4, TI NYLON TUBING	tube, nylon, 1/4, TI NYLON TUBING	SMC	1	30.35
3	SMC AR20-N02-YZ-B	Pressure Regulator	SMC	1	14.90
4	SMC KQ2H07-32A kq2	Bimba Piston Fittings	SMC	2	3.22
5	SY5420-6D-N7T	3 pos, ex center VF3, rated to 100 psi Solenoid Valve	SMC	2	91.05
6	SMC KQ2H07-35AS	kq2 1/4, KQ2 FITTING	SMC	15	21.80
7	SMC ANB1-02	silencer, high noise reduction, AN SILENCER	SMC	2	7.35
8	B094YJJZWV	Air Tank, 13/3000 HPA	Amazon	1	49.99
9	5108N6	Return Spring	McMaster	1	9.41
10	N/A	Sheet metal parts	Sendcutsend	1	30.00
TOTAL =					766.09

4. Testing, Results, and Discussion

4.1 Test Results

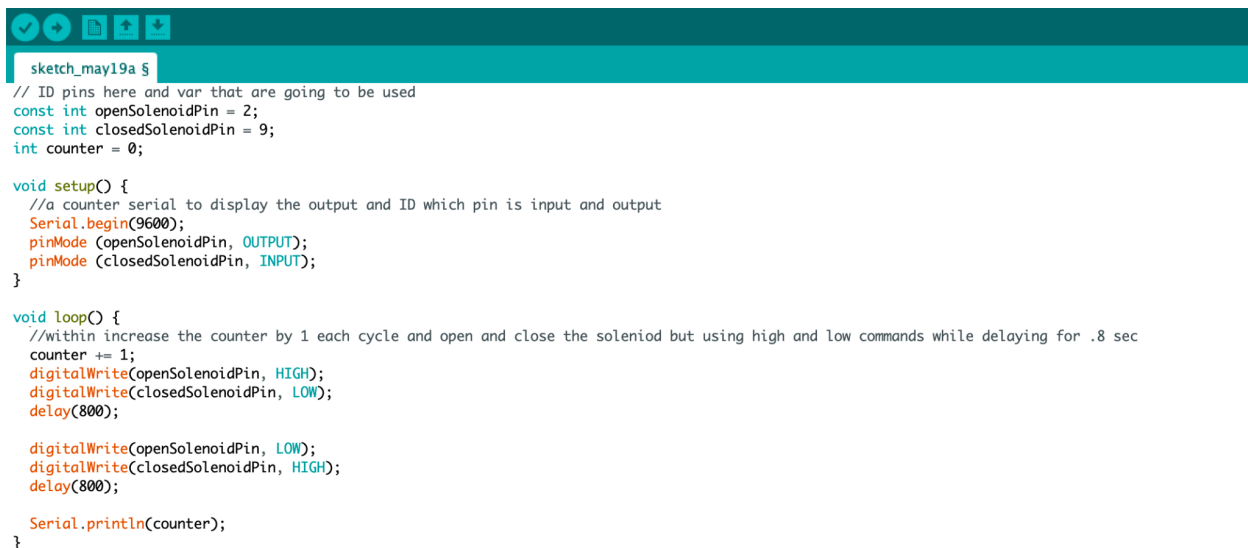
When performing the first track test on the vehicle with all aerodynamic components installed including DRS, several suspension failures occurred. The failures significantly reduced the amount of run time the vehicle had on the track and DRS was only observed for several laps. During the run time that DRS did experience on the track, it handled well and in Figure 46, the driver accelerated through a straight section where the DRS airfoils opened. The drag reduction system withstood the shake-down tests and actuated in a preferable manner. Parameters analyzed by the algorithm throughout track testing were throttle pedal position, steering angle, vehicle speed, and slip ratio.



Figure 46: Driver Accelerating Through Straight Track Section with DRS Actuated

4.2 Actuation Limit

Using Arduino Uno the team was able to test how many actuations the team can accomplish with the specified bottle pressure and an estimate of lines' length that the team is planning to use. After the team pressurized the bottle up to 3000 psi with an output valve set to 80 psi, the team wrote an Arduino code that was able to actuate the Bimba piston continuously. Within Arduino the team used a counter to count the number of full cycles that the Bimba can go through with the amount of pressure that the bottle has. The Arduino code itself is simple where it opens and closes the pneumatic piston till it's physically stopped, After identifying the pins that are being used on Arduino the team had to just open and close the Bimba while introducing a counter to the equation to count the number of cycles that the Bimba will go through.



```
sketch_may19a 5
// ID pins here and var that are going to be used
const int openSolenoidPin = 2;
const int closedSolenoidPin = 9;
int counter = 0;

void setup() {
  //a counter serial to display the output and ID which pin is input and output
  Serial.begin(9600);
  pinMode (openSolenoidPin, OUTPUT);
  pinMode (closedSolenoidPin, INPUT);
}

void loop() {
  //within increase the counter by 1 each cycle and open and close the soleniod but using high and low commands while delaying for .8 sec
  counter += 1;
  digitalWrite(openSolenoidPin, HIGH);
  digitalWrite(closedSolenoidPin, LOW);
  delay(800);

  digitalWrite(openSolenoidPin, LOW);
  digitalWrite(closedSolenoidPin, HIGH);
  delay(800);

  Serial.println(counter);
}
```

Figure 47: Arduino code setup

After the Arduino code had been set up, the team continued to complete the circuit using an H-bridge to supply 12V to the solenoid valve to open and close the piston while getting commands from the Arduino. This allowed us to fully control the solenoid and the Bimba using Arduino Uno helped us complete the test and the results we accounted for are 103 full cycle actuation

with an estimate of two 50in air lines that attach to the solenoid from one side and the other side attaches to the Bimba and another 12.5in air line that attaches to the solenoid and the other end attaches to the air bottle supplying the solenoid with air pressure. During the testing, the team monitored and measured temperature, number of actuation, the temperature of the piston, and the time till the bottle ran out of pressure after continuous actuation. Within testing, there is a 0.8s delay between each open and close of the piston to avoid any overheating issues.

Table 4: Max number of actuation results

Output pressure (psi)	80
Line length (solenoid to bottle) (In)	12.5
Line length (solenoid to piston) (In)	50
Delay(sseconds)	0.8
Number of accuations	103
Piston temp (F)	84.3
Time of testing till empty(minutes)	3.34

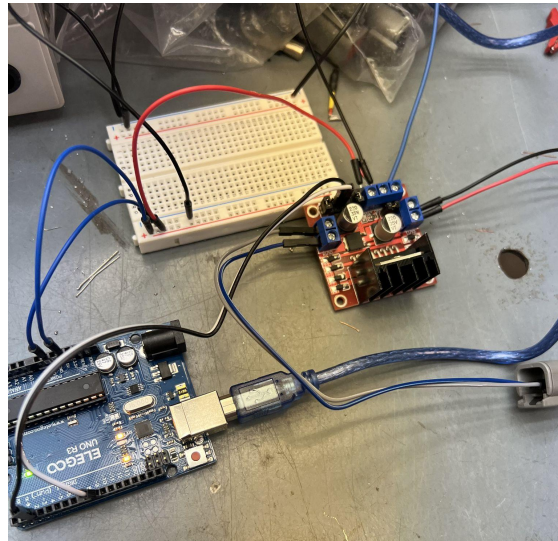


Figure 48: Circuit setup for testing

4.3 Lap Simulation

With manufacturing and personnel challenges affecting the entire vehicle, theoretical and semi-functional testing had become more important. The previously recorded data from the endurance test in Michigan could expose the DRS to real-world parameter value combinations. The intention to create a lap simulator that could broadcast the recorded race data from i2 Pro to the ECU to control the DRS was first attempted with an Arduino Nano microcontroller. The Nano did not have the capability to analyze the large .CSV files that were exported containing the race data, even after the sampling frequency was reduced to 10Hz. Next, an Adafruit FM4E was used to transfer the data using Python and leave the .CSV files on a host desktop. The FM4E proved to be challenging regarding hardware as the microcontroller is 3.3V based and the sensor data to transfer needed a range of 0V to 5V. Rather than use several transistors on a breadboard, an additional Arduino to piggyback off of the FM4E, the National Instruments myDAQ was selected.

The lap simulator was successfully created with LabVIEW and the myDAQ. The VI could quickly parse through the hundreds or thousands of elements in the saved data .CSV files and output them as analog voltages. The myDAQ analog outputs were able to emulate two sensors for the DRS. As shown in Figure 49, the VI in LabVIEW ran off while loops and matched the ECU sampling rate of 10Hz. Critical features for the VI to operate were the use of the shift register function on the inner case structure and DAQ assist outputs. The developed algorithm and assembled rear wing with DRS were tested successfully and the operation was found to be satisfactory with the lap simulator. Manual trigger, constant on, and fully autonomous modes behaved well and system air pressure was tuned during the testing exercises. The recorded parameters that were used were the baseline minimum sensors of throttle pedal position steering angle. The NI myDAQ is limited to two analog outputs but a remaining PWM digital out pin could be set up for the addition of one more sensor.

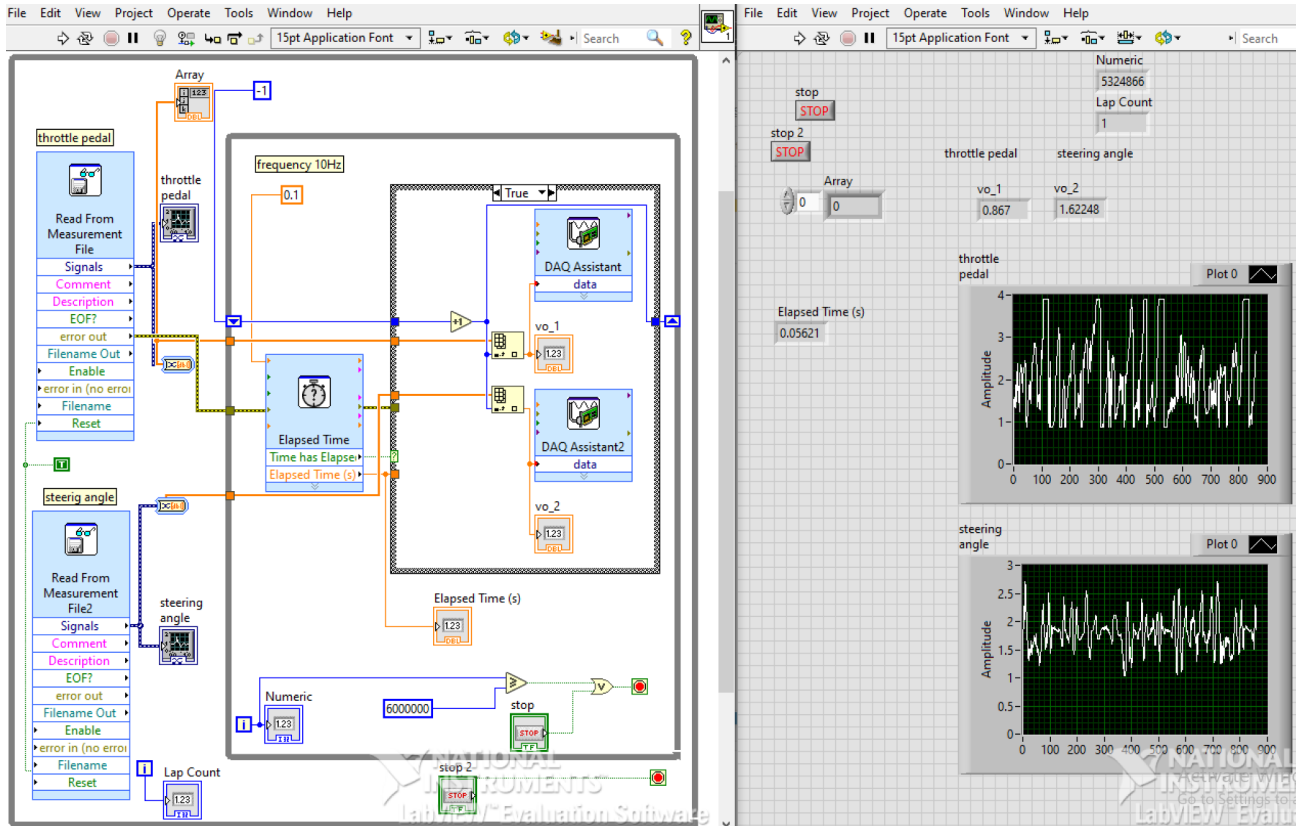


Figure 49: LabVIEW VI for the DRS Lap Simulator

4.4 Social Impacts

The drag reduction system project provides students participating in the Formula SAE team with hands-on knowledge of designing, manufacturing, testing, and validating a project. The project improves the real-life problem-solving skills of the project contributors. The members of the Formula SAE team get to work on their passion and make meaningful connections through the team projects. On top of that, the team members learn a lot of really good skills that can be applied in future careers. The project also provides the Formula SAE team members with industry knowledge by connecting the team members with working engineers during the competitions. The design review

process of the drag reduction system project prepares the team members for the actual design review process in the automotive industry. The Formula SAE team projects also utilize several workplace products and communication software. All in all, the drag reduction system project helps the team members to adapt to the workspace standards. Ultimately, the project provides better job opportunities to the team project members who have hands-on experience in engineering.

5. Conclusions and Future Work

The main purpose of the Drag Reduction System (DRS) is to allow the driver to adjust the aerodynamics of the car leading to reducing the amount of drag that is being exerted on the car in a straight line allowing the driver to go faster. Throughout the semester the team managed to assemble the entire rear wing with the drag reduction system attached to it. The team also designed a failsafe mechanism where under extreme conditions mid-race that the pneumatic system fails the flaps would close by the spring that is mounted to the piston allowing it to close the flaps and not sacrifice the downforce that is needed when taking sharp corners.

While our design should work properly throughout the competition there is definitely room for improvements such as relocating the mounting of the piston for better aerodynamic flow, reconsidering servo motors, re-run CFD data on the flaps, and considering adding DRS to the front wing of the car to help with downforce and turning around sharp corners. Moving forward, the team is going to implement the design of the DRS on the Spartan Racing combustion (SR 13) and electric team's (SRE 6) vehicle with the support and the calibration of the Powertrain team, aerodynamic, and vehicle dynamics team.

References

Benson, T. (n.d.). Inclination Effects on Lift and Drag. NASA Glenn Research Center.

Retrieved May 3, 2022, from <https://www.grc.nasa.gov/www/k-12/VirtualAero/BottleRocket/airplane/kiteincl.html>

Encyclopaedia Britannica. (n.d.). Hooke's law | Description & Equation. Retrieved May

9, 2022, from <https://www.britannica.com/science/Hookes-law>

Golson, J. (2014, May 7). An Inside Look at the Insanely Complex Formula 1 Steering

Wheel. Wired. Retrieved May 1, 2022, from <https://www.wired.com/2014/05/formula-1-steering-wheels/>

Huang, L. (2021, August 2). 6061 vs. 7075 Aluminum: Which One Should You Choose

for Your Projects? Rapid Direct. Retrieved May 18, 2022, from <https://www.rapiddirect.com/blog/6061-vs-7075-aluminum/>

Huang, L. (2021b, August 3). 4140 vs 4130 Steel: The Right Steel for Your Project.

Rapid Direct. Retrieved May 18, 2022, from <https://www.rapiddirect.com/blog/4140-vs-4130-steel/>

Keim, R. (n.d.). Potentiometer. EE Power. Retrieved May 6, 2022, from

<https://eepower.com/resistor-guide/resistor-types/potentiometer/#>

Kemble, J. (2022, March 21). What does DRS mean in F1? Meaning of Formula 1 term,

what it stands for, how it works, when it was introduced. NationalWorld.

Retrieved May 1, 2022, from <https://www.nationalworld.com/sport/other-sport/what-does-drs-mean-in-f1-meaning-of-formula-1-term-what-is-stands-for-how-it-works-when-it-was-introduced-3620304>

MoTeC Pty Ltd. (n.d.). MoTeC M1 Build Get Started. MoTeC. Retrieved May 1, 2022, from https://www.motec.com.au/filedownload.php/m1_build_get_started.pdf?docid=4875

MoTeC Pty Ltd. (n.d.). MoTeC M1 GPA. MoTeC. Retrieved May 1, 2022, from <https://www.motec.com.au/gpa-m1/gpa-m1-ov/>

MoTeC Pty Ltd. (n.d.). MoTeC M1 Tune User Manual. MoTeC. Retrieved May 1, 2022, from: https://www.motec.com.au/filedownload.php/M1_tune_user_manual.pdf?docid=4131

MoTeC Pty Ltd. (n.d.). MoTeC M150 ECU Datasheet. MoTeC. Retrieved May 1, 2022, from: <https://www.motec.com.au/filedownload.php/CDS13150%20M150%20ECU.pdf?docid=3717>

PresticeBDT. (2021, April 23). How F1 DRS works - Aero of Formula One DRS explained. Retrieved May 1, 2022, from: <https://www.presticebd.com/how-f1-drs-works-the-aerodynamics-of-formula-one-drs-explained/>

Ryan, V. (2003). Pop Riveting. ENGINEERING - DESIGN AND TECHNOLOGY. Retrieved May 14, 2022, from <https://www.technologystudent.com/joints/>

[popriv1.htm](#)

SAE International. (2021). Formula SAE Rules 2022. Formula SAE® Rules 2022.

Retrieved May 14, 2022, from <https://fsaeonline.com/cdsweb/gen/Download>

[Document.aspx?DocumentID=42f9ab71-0a41-4a92-a5d4-aa3d284e5c05](https://fsaeonline.com/cdsweb/gen/DownloadDocument.aspx?DocumentID=42f9ab71-0a41-4a92-a5d4-aa3d284e5c05)

Stoops, S. (2013, February). Understanding Angle of Attack. Model Aviation. Retrieved

May 3, 2022, from <https://www.modelaviation.com/angle-of-attack>

Appendix

Appendix A: Simulations

Table 5: Rear Wing Drag and Downforce Analysis at different AoA

Inlet Velocity, mph	AoA, degree	Drag, lbf/m-span	Downforce, lbf/m-span	L/D Ratio
35.0 mph	-5.0 deg	8.947992698056042 lbf	47.05765491675751 lbf	5.259018028
35.0 mph	-4.5 deg	9.546568352894324 lbf	44.72905394386476 lbf	4.685354181
35.0 mph	-4.0 deg	10.102911130657017 lbf	42.620029114356726 lbf	4.218588936
35.0 mph	-3.5 deg	10.348662825783276 lbf	41.759536951451366 lbf	4.035259207
35.0 mph	-3.0 deg	10.657800141839516 lbf	41.187041628829874 lbf	3.864497465
35.0 mph	-2.5 deg	10.940276285257342 lbf	41.268303833054226 lbf	3.772144575
35.0 mph	-2.0 deg	10.999078883677667 lbf	41.538266310495466 lbf	3.776522266
35.0 mph	-1.5 deg	11.412722255797403 lbf	40.648454129332485 lbf	3.561679082
35.0 mph	-1.0 deg	11.59584178245736 lbf	39.37401563964847 lbf	3.395528878
35.0 mph	-0.5 deg	11.903659072971486 lbf	39.28447296161352 lbf	3.300201452
35.0 mph	0.0 deg	12.0722126717058 lbf	38.48674880015904 lbf	3.1880443
35.0 mph	0.5 deg	12.350436290117095 lbf	37.83063171063431 lbf	3.063100835
35.0 mph	1.0 deg	12.551055541536842 lbf	37.724841490942396 lbf	3.005710664
35.0 mph	1.5 deg	12.778607400469488 lbf	37.219967250817575 lbf	2.912677891
35.0 mph	2.0 deg	12.986478918284222 lbf	36.9357189509326 lbf	2.844167321
35.0 mph	2.5 deg	13.215101401888417 lbf	36.54053122225005 lbf	2.765058709
35.0 mph	3.0 deg	13.403167092970135 lbf	35.96653901700236 lbf	2.683435845
35.0 mph	3.5 deg	13.604006076618965 lbf	35.980732318808435 lbf	2.644863
35.0 mph	4.0 deg	14.359226616738084 lbf	38.63565457292421 lbf	2.690650103
35.0 mph	4.5 deg	13.881772088254474 lbf	34.30289909507832 lbf	2.471074937
35.0 mph	5.0 deg	14.986263668121104 lbf	39.22453910348966 lbf	2.617366141

Table 6: CFD results of different rear wing configurations at 55 mph

	Half Car DF (lbs)	Half RW DF (lbs)	Full Car DF (lbs)	Full Car DF (N)	Full RW DF (lbs)	Half Car Drag (lbs)	Half RW Drag (lbs)	Full Car Drag (lbs)	Full Car Drag (N)	RW Drag (lbs)	CoP (%F)	
Base-line	127.9	55.78	255.8	1137.8	55089	61.3	25.55	122.6	545.351	97	51.1	51.7

Top Flap Open	107.54	38.78	215.08	956.72 3505	77.56	44.38	13.99	88.76	394.824 1506	27.9 8	67.3 8
Middle Flap Open	104.32	36.2	208.64	928.07 69578	72.4	44.22	14.55	88.44	393.400 7197	29.1	68.2 7
Bottom Flap Open	105.08	37.05	210.16	934.83 82547	74.1	45.8	16.17	91.6	407.457 1	32.3 4	66.2
Upper 2 Flaps Open	93.03	27.24	186.06	827.63 61137	54.48	38.8	9.05	77.6	345.181 9973	18.1	79.4 5
Middle Flap Closed	96.58	30.2	193.16	859.21 84872	60.4	41.54	11.325	83.08	369.558 2518	22.6 5	
Lower 2 Flaps Open	96.05	29.91	192.1	854.50 33723	59.82	39.79	11.6	79.58	353.989 4761	23.2	74.2 9
All Flaps Open	82.25	19.19	164.5	731.73 24557	38.38	34.4	6.395	68.8	306.037 6471	12.7 9	89.9

Appendix B: Hardware

Voltage (V)	Distance (cm)
-10.7048	0
-10.1718	0.5
-9.5546	1
-9.01864	1.5
-8.3352	2
-7.83254	2.5
-7.25	3

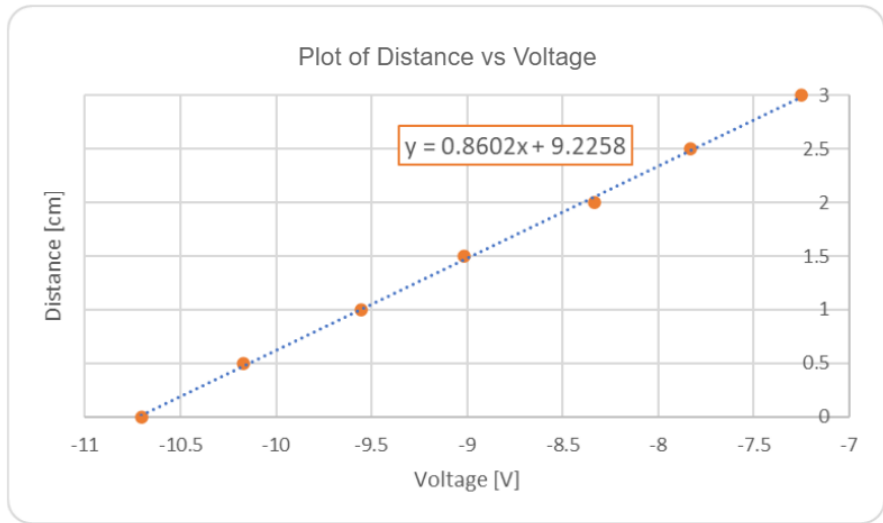


Figure 50: Calibration analysis of the throttle position sensor

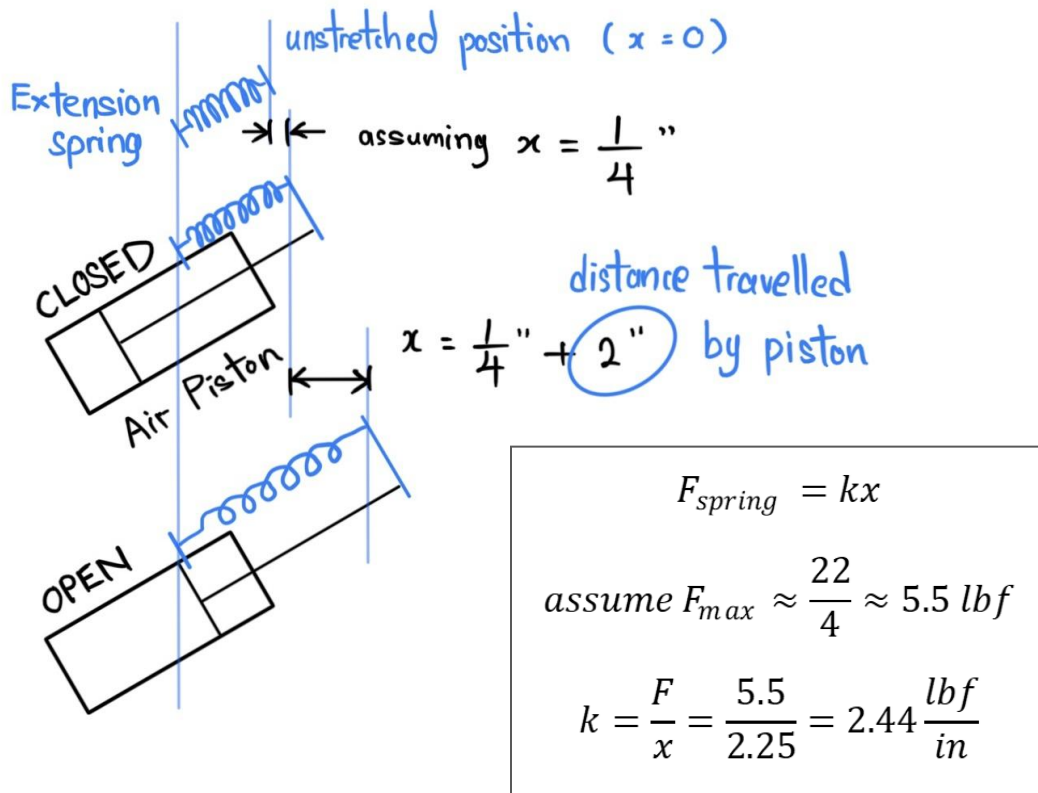


Figure 51: Return spring constant analysis and calculation

Table 7: Decision matrix for actuation method analysis

actuation types	system cost	additional energy source required?	actuation time	system weight	CG position(x,y,z) inches	effect on aero (10 = little interference)	durability (1 = weak)	"fail safe" capable system (1 = no)	design time (10 is efficient)	total
Category weight (multiplier)	5	3	10	10	0	8	8	10	7	
hydraulic	5	~	~	1	~	5	8	9	1	~
stepper motors	8	10	5	3	1	5	5	1	5	275
Screw type linear actuator	10	10	1	2	1	5	8	1	10	294
servo	1	10	8	10	5	7	8	3	1	372
manual trigger, pneumatic linear	8	1	10		10	7	9	1	10	351
pneumatic, linear	5	1	10	8	10	7	10	10	9	507
pneumatic, rotary	8	1	10	7	7	6	7	10	5	452

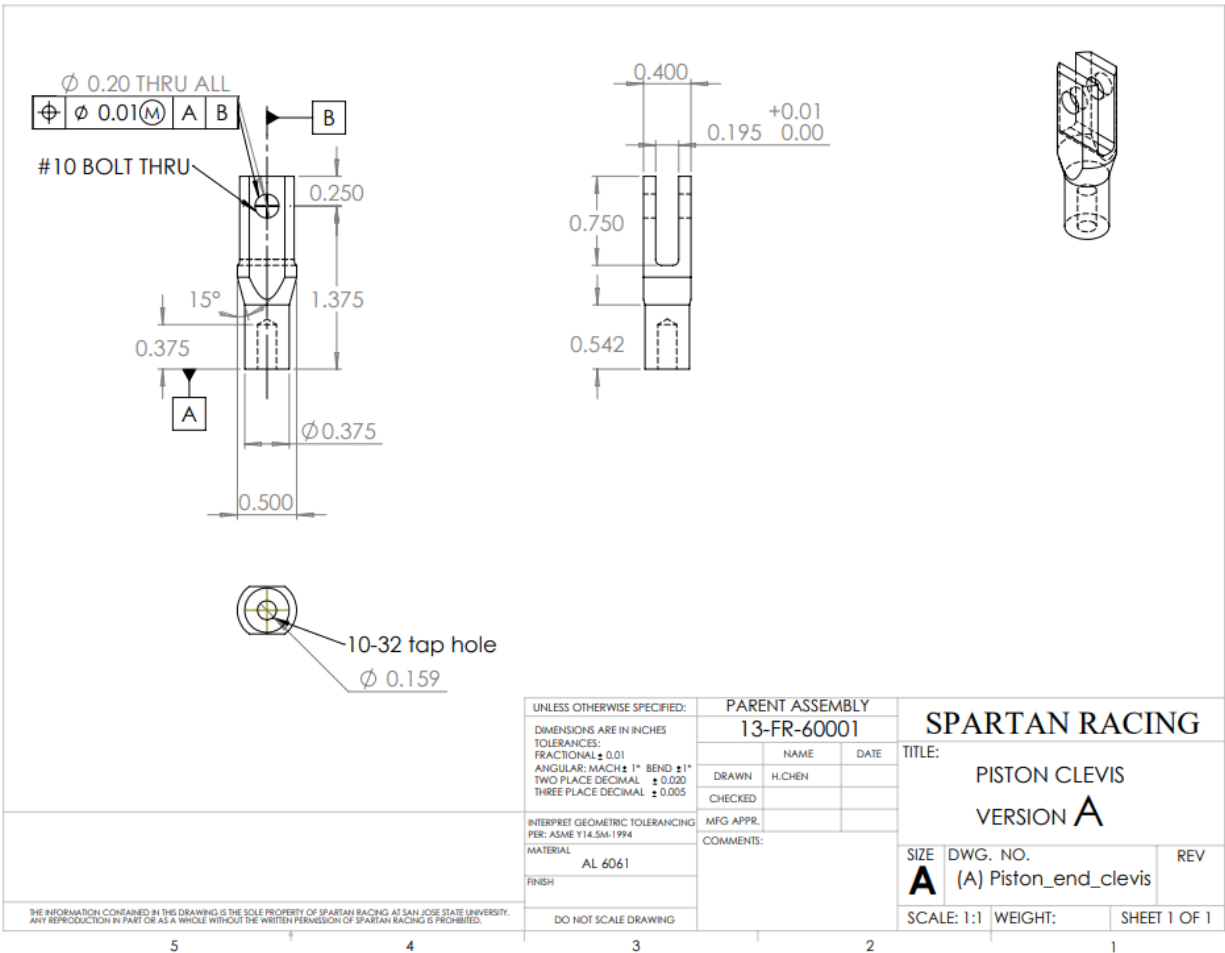


Figure 52: SolidWorks drawing of the piston clevis

Table 8: Piston selection analysis

Manufacturer	Bimba	SMC	SMC	SMC	SMC
part #	022-DXPB	NCDGBA20-2200-X142US	NCDGCA32-0200	NCDGLN20-0200-M9NW	NCDGCA20-0200
cost	36.33	72.8	56.85	123.6	46.6
max force at 100psi	22.6 lbf	40.9 lbf	107 lbf	40.9 lbf	40.9 lbf
piston stroke	2in	2in	2in	2in	2in
mass	68g	322.05g	470g	68g	210g
damping	internal rubber bump stop	internal urethane cushion	air cushion	internal urethane cushion	air cushion
air line ports threads	10-32 UNF	10-32 UNF	1/8in NPT	10-32UNF	
piston head thread	10-32	M8x1.25	M10x1.25	M8x1.25	
source	TSI	SMC	SMC	SMC	SMC
mount	rear clevis	basic style	rear clevis	axial foot style	rear clevis
position sensor	yes	yes	yes	yes	yes
bore OD	15mm	20mm	32mm	20mm	20
effective area (bore ID - piston OD)					
	0.226 in^2	2.64x10^-4 m^2 0.409 in^2	6.91x10^-4 m^2 1.07 in^2	2.64x10^-4 m^2 0.409 in^2	

Table 9: Sensor validation and analysis

Inputs	Calculated Val?	Derived from	Accuracy	Range	Threshold	Importance
Front Brake Pressure	no	N/A	±1 %Span	0psi - 15kpsi	50psi	show system driver intends to slow down
Throttle Pedal Position	no	N/A	±0.1 %	10mm - 150mm	95%	when driver wants to accelerate
Steering angle	no	N/A	± 0.5 %	360° continuous	15deg	avoid DRS open in turns
Steering rate	yes	Steering angle			too noisy	avoid DRS open in slaloms
Average wheel Speed	yes	Individual wheel speed measurements			30mph	low drag below ~30mph, negligible gain
Slip ratio	yes	Individual wheel speed measurements			0.2	use DRS when car has grip
G force lat	Can be	Daq internal IMU			-/+ 0.50	maintain downforce when G's are higher

Table 10: 4-bar linkage calculations

Transmission angle taken from the two endpoints and midpoint normalized by sin operation.
The average overall transmission is analyzed against the length of the pneumatic piston.

Total = sum(cos(radians(abs(A.F))))

	Piston length (inches)	Degrees						abs(cos(radians(angle)))					
		A (deg)	B (deg)	C (deg)	D (deg)	E (deg)	F (deg)	A	B	C	D	E	F
	5.25	129.1	108.48	91.46	132.49	107.26	83.93	0.7760464071	0.9484343576	0.9996753563	0.7373952383	0.9549681736	0.9943934476
	5.5	124.59	104.93	88.49	130.78	105.24	81.69	0.8232354634	0.9062413124	0.999652741	0.7572230963	0.9648332167	0.9895005791
	5.75	120.03	101.24	85.34	129.06	103.21	79.44	0.8657634857	0.8808193151	0.9966943478	0.7764865127	0.9735390333	0.9830635319
(A) best down stroke	6	115.43	97.45	82.05	127.36	101.17	77.17	0.9031105791	0.9915583894	0.9903891431	0.7948384552	0.9810567217	0.9750332181
	6.25	110.83	93.57	78.65	125.66	99.13	74.9	0.9346396147	0.9980594687	0.9804432899	0.8124907176	0.98733086	0.9654726309
	6.5	106.24	89.66	75.18	123.99	97.11	72.63	0.9600986791	0.9999823932	0.9667341623	0.8291351575	0.9923103502	0.9543967751
(B) best avg	6.75	101.7	85.75	71.69	122.36	95.09	70.36	0.9792228106	0.9972501851	0.9493706612	0.8447017974	0.9960565652	0.9418230339
	7	97.24	81.87	68.2	120.76	93.1	68.12	0.9920269604	0.9899497463	0.9284858269	0.8593171609	0.9985366703	0.9279663947
(C) best up stroke	7.25	92.9	78.06	64.77	119.21	91.15	65.9	0.9987193572	0.978364789	0.9046039909	0.8728369164	0.9997985785	0.9128341772
	7.5	88.69	74.36	61.42	117.73	89.23	63.72	0.9997386344	0.9629745906	0.8781500169	0.8851501137	0.999096975	0.8966410368
	7.75	84.65	70.79	58.18	116.31	87.36	61.57	0.9956437105	0.9443189578	0.8497086989	0.8964090862	0.998938657	0.879399416
	8	80.79	67.36	55.08	114.96	85.54	59.47	0.9871083455	0.9229417034	0.8199521093	0.9066026094	0.9969718656	0.8613632959

Table 11: 4-bar linkage calculations

sum(A:F)/6		avg(A+B+D+E)		avg(B+C+D+E)		
Avg Efficiency	%different	up stroke	%different	down stroke	%different	Piston length (inches)
0.9018188301	-4.958534551	0.8542110442	-10.77322149	0.9743678338	-1.014153431	5.25
0.9167810682	-3.462310742	0.8778832722	-8.405998686	0.9800569623	-0.4452405779	5.5
0.9293943711	-2.200980451	0.8991520867	-6.279117239	0.983529057	-0.09803110672	5.75
0.9393310845	-1.207309114	0.9176410364	-4.430222271	0.9845093681	0	6
0.946406097	-0.4998078642	0.9331301652	-2.881309386	0.9828265624	-0.168280573	6.25
0.9504429196	-0.09612560234	0.945381645	-1.656161409	0.9783559202	-0.6153447895	6.5
0.9514041756	0	0.9543078396	-0.7635419518	0.9711251113	-1.338425677	6.75
0.9493804599	-0.2023715675	0.9599576345	-0.1985624599	0.9612346595	-2.327470856	7
0.9445263015	-0.6877874064	0.9624299103	0.04866511643	0.9489003839	-3.560898419	7.25
0.937094015	-1.431016061	0.9619432591	0	0.9344188355	-5.009053263	7.5
0.9274030878	-2.400108785	0.9588276029	-0.3115656217	0.9180914324	-6.641793565	7.75
0.9158233215	-3.558085409	0.953406131	-0.853712814	0.9003072435	-8.420212456	8

Appendix C: Software

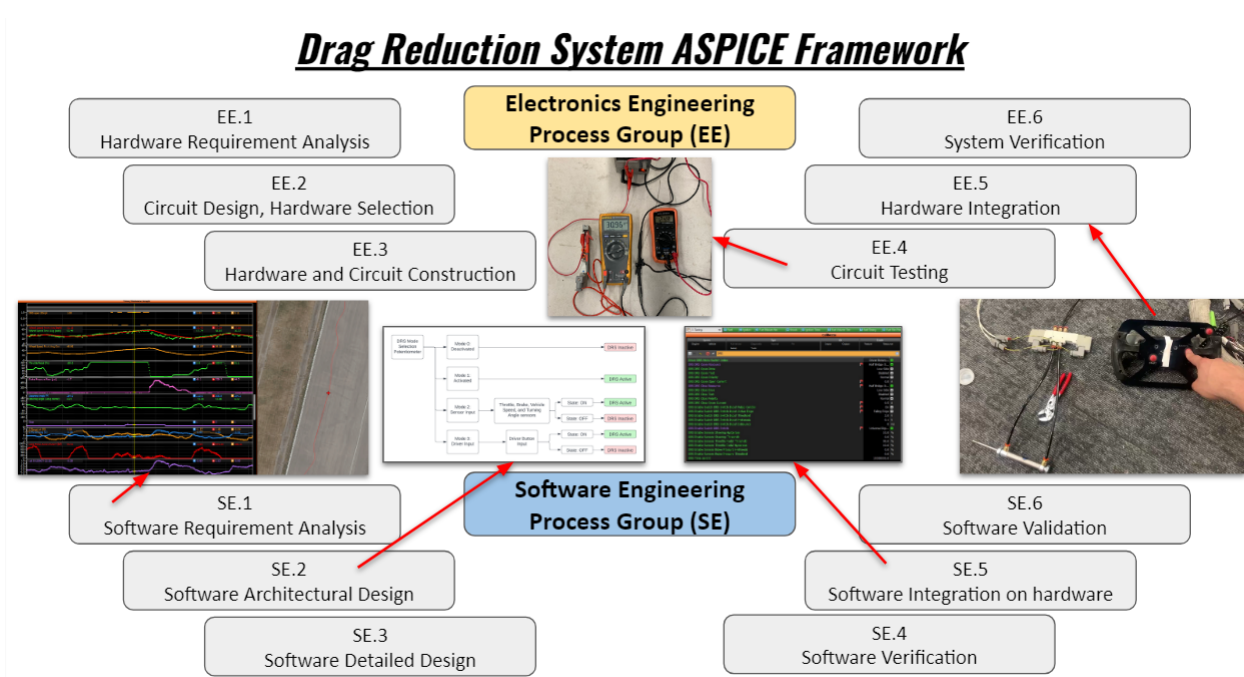


Figure 53: Automotive Software Process Improvement and Capability Determination (ASPICE) Framework of Drag Reduction System

System	Type	I/O	Enable
Engine Vehicle	Advanced Pin Diagnostic Setup Normal Tune	Input Output	Feature Resource
drs			
Driver DRS Mode Switch	~		
Driver DRS Mode Switch Index		Driver Rotary Switch 3	<input checked="" type="checkbox"/>
DRS DRS Open Resource		Half Bridge Output 4	<input checked="" type="checkbox"/>
DRS DRS Open State	~		
DRS DRS Open Drive		Low Side	<input type="checkbox"/>
DRS DRS Open Test		Disabled	<input type="checkbox"/>
DRS DRS Open Polarity		Normal	<input type="checkbox"/>
DRS DRS Open Open Current		0.0 A	
DRS DRS Open Output Duty Cycle	~	%	
DRS DRS Open Voltage	~	V	
DRS DRS Open Voltage Absolute	~	V	
DRS DRS Open Pin Diagnostic	~		
DRS DRS Close Resource		Half Bridge Output 7	<input checked="" type="checkbox"/>
DRS DRS Close State	~		
DRS DRS Close Drive		Low Side	<input type="checkbox"/>
DRS DRS Close Test		Disabled	<input type="checkbox"/>
DRS DRS Close Polarity		Normal	<input type="checkbox"/>
DRS DRS Close Open Current		0.5 A	
DRS DRS Close Output Duty Cycle	~	%	
DRS DRS Close Voltage	~	V	
DRS DRS Close Voltage Absolute	~	V	
DRS DRS Close Pin Diagnostic	~		
DRS Enable Switch DRS Switch Input	~		
DRS Enable Switch DRS Switch Input Voltage	~	V	
DRS Enable Switch DRS Switch Input Diagnostic	~		
DRS Enable Switch DRS Switch Input Pullup Control		On	<input type="checkbox"/>
DRS Enable Switch DRS Switch Input Active Edge		Falling Edge	<input type="checkbox"/>
DRS Enable Switch DRS Switch Input Threshold		3.0 V	

Figure 54: M1 Tune

Group	Type	Unit
DRS	Group	
DRS Open	Switched Output	
DRS Close	Switched Output	
Timer	Timer	
Enable	Group	Mode Enumeration
Switch	Group	
Sensors	Group	
Steering	Group	Mode Enumeration
Hysteresis	Parameter	Floating Point
Threshold	Parameter	Floating Point
Update	Scheduled Function	
Value	Channel	Mode Enumeration
Throttle Pedal	Group	Mode Enumeration
Value	Channel	Mode Enumeration
Threshold	Parameter	Floating Point
Hysteresis	Parameter	Floating Point
Update	Scheduled Function	
Brake Pressure	Group	Mode Enumeration
Value	Channel	Mode Enumeration
Update	Scheduled Function	
DRS Solenoid Update Fu...	Scheduled Function	
DRS Solenoid Timer	Parameter	Floating Point
		Unitless

Figure 55: M1 Build

Appendix D: Miscellaneous

Formula SAE Rules Concerning the DRS



T.9.2.3 All aerodynamic devices must be designed such that the mounting system provides adequate rigidity in the static condition and such that the aerodynamic devices do not oscillate or move excessively when the vehicle is moving. Refer to IN.8.2

IN.8.2.1 Any aerodynamic devices may be checked by pushing on the device in any direction and at any point. The following is guidance but actual conformance will be up to technical inspectors at the respective competitions. The intent is to reduce the likelihood of wings detaching.

IN.8.2.2 If any deflection is significant, then a force of approximately 200 N may be applied and the resulting deflection should not be more than 25 mm and any permanent deflection less than 5 mm.

IN.8.2.3 If any vehicle on track is observed to have large, uncontrolled movements of aerodynamic devices, then officials may Black Flag the vehicle for IN.15 Reinspection.

IN.15.2.1 The Inspection process may be repeated in entirety or in part IN.15.2.2 Specific areas or items to be inspected are at the discretion of the Chief Technical Inspector.

Figure 56: Formula SAE rules concerning the Drag Reduction System

Appendix E: MoTeC Code

```
local hyst = Calculate.Hysteresis(Throttle.Pedal , Threshold
- Hysteresis, Threshold, 0.0);

Value = hyst
    ? Value.Enabled
    : Value.Disabled;

// Compare the value of Enable with the current state of the
actuators

// Static local variable to track state of actuator
// States are
// 0 - Closing - DRS is deactivating
// 1 - Closed - DRS is disabled
// 2 - Open - DRS is active
// Start in the closed / disabled state
static local drsState = 1;

// Local variables representing the state of the solenoid
valves
// TRUE -> Open
// FALSE -> Closed
local OPEN = true;
local CLOSED = false;

// Check whether DRS should be enabled or disabled based on
DRS mode / driver input
```



```

when (Root.DRS.Enable) {
  is (Enabled) {
    // Check if actuator was closing or closed
    if (drsState eq 0 or drsState eq 1) {
      // Deactivate the close valve
      DRS Close.SetState(CLOSED);
      // Activate the open valve
      DRS Open.SetState(OPEN);
      // Update the state
      drsState = 2;
    }
  }
  is (Disabled) {
    // Check if solenoid was open
    if (drsState eq 2) {
      // Deactivate the open valve
      DRS Open.SetState(CLOSED);
      // Activate the close valve
      DRS Close.SetState(OPEN);
      // Start the timer
      Timer.Start(DRS Solenoid Timer);
      // update the state
      drsState = 0;
    }
    // Check if actuator was closing

```

```

else if (drsState eq 0) {
    // if timer has finished, close both solenoids
    if (Timer.Remaining() <= 0 ) {
        DRS Close.SetState(CLOSED);
        DRS Open.SetState(CLOSED);
        drsState = 1;
    }
}

}

// Local variable to determine state of DRS
// 0 -> DRS should not be active
// 1 -> DRS should be active
// Default to DRS inactivity
local drsIsActive = 0;

local switchValue = Driver.DRS Mode Switch.AsInteger();

if (switchValue eq 0 ) {
    drsIsActive = 0;
}

else if (switchValue eq 1) {
    if (DRS.Enable.Switch.DRS Switch Input.AsInteger() eq 1)
    {
        drsIsActive = 1;
    }
}

```

```

    }
}
else if (switchValue eq 2) {
    //if (DRS.Enable.Sensors.Throttle Pedal.AsInteger() eq 1
and DRS.Enable.Sensors.Steering.AsInteger() eq 1) {
        //    drsIsActive = 1;
        //}
        if (DRS.Enable.Sensors.Throttle Pedal.AsInteger() eq 1
and
        DRS.Enable.Sensors.Steering.AsInteger() eq 1 and
        //DRS.Enable.Sensors.Brake Pressure.AsInteger() eq 1 and
        DRS.Enable.Sensors.Wheel Speed.AsInteger() eq 1 and
        DRS.Enable.Sensors.Slip Ratio.AsInteger() eq 1 ) {
            drsIsActive = 1;
        }
        else {
            drsIsActive = 0;
        }
    }
else if (switchValue eq 3) {
    drsIsActive = 1;
}
else {
    drsIsActive = 0;
}
}

```

```

DRS.Enable.Value.Set(drsIsActive);

/*
local on = true;

//mode zero = disabled
    if (Driver.DRS Mode Switch.AsInteger() eq 0)
    {
        on = true;// true equal close
    }
//mode 1 = manual
    else if (Driver.DRS Mode Switch.AsInteger() eq 1)
    {
        if (Root.DRS.Enable.Switch.DRS Switch
Input.AsInteger() eq 1)
        {
            on = false;
        }
        if (Root.DRS.Enable.Switch.DRS Switch
Input.AsInteger() eq 0)
        {
            on = true;
        }
    }
//mode 2 = auto

```

```
        else if (Driver.DRS Mode Switch.AsInteger() eq 2)
        {
            on = Sensors.Throttle Pedal eq Sensors.Throttle
Pedal.Enabled;

        }
//mode 3 = always open (thats what she said)
        else if (Driver.DRS Mode Switch.AsInteger() eq 3)
        {
            on = false;
        }

Value = on
    ? Value.Disabled
    : Value.Enabled;

*/
```